

Simultaneous ground-state cooling of two levitated nanoparticles by coherent scattering

Yi Xu,¹ Yu-Hong Liu,¹ Cheng Liu,¹ and Jie-Qiao Liao^{1,2,*}

¹Key Laboratory of Low-Dimensional Quantum Structures and Quantum Control of Ministry of Education, Key Laboratory for Matter Microstructure and Function of Hunan Province, Department of Physics and Synergetic Innovation Center for Quantum Effects and Applications, Hunan Normal University, Changsha 410081, China

²Institute of Interdisciplinary Studies, Hunan Normal University, Changsha, 410081, China

(Dated: May 21, 2024)

Simultaneous ground-state cooling of two levitated nanoparticles is a crucial prerequisite for investigation of macroscopic quantum effects such as quantum entanglement and quantum correlation involving translational motion of particles. Here we consider a coupled cavity-levitated-particle system and present a detailed derivation of its Hamiltonian. We find that the y -direction motions of the two particles are decoupled from the cavity field and both the x - and z -direction motions, and that the z -direction motions can be further decoupled from the cavity field and the x -direction motions by choosing proper locations of the particles. We study the simultaneous cooling of these mechanical modes in both the three-mode and five-mode cavity-levitated optomechanical models. It is found that there exists a dark-mode effect when the two tweezers have the same powers, which suppress the simultaneous ground-state cooling. Nevertheless, the simultaneous ground-state cooling of these modes can be realized by breaking the dark-mode effect under proper parameters. Our system provides a versatile platform to study quantum effects and applications in cavity-levitated optomechanical systems.

I. INTRODUCTION

With the development of micro- and nano-fabrication techniques, great advances have recently been achieved in cavity optomechanics, especially on the fundamentals of quantum physics and modern quantum technology [1, 2]. The optically levitated particles, as a kind of novel optomechanical platform, have attracted much attention from the communities of quantum optics and quantum information [3–5]. In 1970s, it has been discovered that the particles can be levitated by focusing beams of light [6–8], and this discovery has played a crucial role in advancing the field of atom trapping and cooling [9]. In recent years, much attention has been paid to quantum manipulation of the translation and rotation of the center-of-mass of particles, and great advances have been made in this platform, such as the realization of a controllable torque induced by the spins of atoms embedded in a microscale object [10], the measurement of the Brownian motion of micrometer-sized beads [11], and the cooling of the motion of particles into the quantum ground state [12–14]. The levitated particles can also be utilized for quantum precision measurements, including acceleration measurement [15, 16], mass measurement [17], and gyroscope [18, 19].

Levitated nanoparticles were conceived as a candidate to explore macroscopic quantum phenomena [20–28]. This is because the nanoparticles are considered as a kind of macroscopic quantum system, and they can be levitated in a high vacuum [20–22, 29], which reduces the thermal contact between mechanical motion and environment. As a result, these systems have exceptionally high mechanical quality factors, and are considered as an excellent candidate for studying low-dissipation optomechanics. The first step to exploring quantum effects in macroscopic mechanical systems is the cooling

of the mechanical systems to their ground states [30–34]. It has been reported that the levitated particles can be significantly cooled via feedback cooling [22–24, 35–37] and sideband cooling [38–43]. The standard sideband-cooling method in optomechanical systems typically requires an externally red-detuned pumping field to remove the energy from the particles [25, 29, 44]. However, high driving powers will lead to the trapping of cavity fields for the optically levitated systems, and then reducing the cooling rate [29]. In addition, the laser-phase noise can hinder ground-state cooling at the relevant frequencies of the trapped nanoparticles [45–47]. To overcome these challenges, the coherent scattering technique has been introduced into the levitated particle systems [12, 48–51], drawing from atomic physics experiments [52]. This method harnesses higher optical trapping powers and larger particles to achieve stronger coupling strengths [53], thereby paving the way to ultra strong coupling [54] and leading to novel quantum optomechanical effects. These works were mostly based on the cooling of a single particle. In parallel, an increasing amount of research is focusing on the field of multi-levitated particles [55–68]. Compared with other mechanical oscillator arrays, the array of optically levitated particles has better controllability [69–73]. Motivated by these advances, we are committed to study the simultaneous ground-state cooling of multiple levitated particles and to explore more novel quantum effects.

In this paper, we study the simultaneous ground-state cooling of two levitated particles coupled to a cavity field. Similar to a single-particle case, the photon enters the cavity via the scattering process, which provides the mechanism for cooling the center-of-mass motions of the particles. For multiple particles levitated simultaneously, the mechanical effect of the scattered light between the particles has been ignored in the past. However, the recent experimental observations indicate that this scattering effect cannot be neglected for some cases [74–77]. The redistributed light field greatly affects the equilibrium position of the particles. Therefore, we consider

* Corresponding author: jqiao@hunnu.edu.cn

the optical binding effect between the two nanoparticles. In particular, we find that the y -direction motions of the two particles decouple from other degrees of freedom in this system. We also find that, when the two nanoparticles are located at the cavity nodes, the cavity mode only couples to the x modes of the particles. Benefiting from the extremal isolation of the system, the simultaneous ground-state cooling of the center-of-mass motions of the two nanoparticles along x -axis can be realized. When the two nanoparticles are not located at the specific positions, both the x mode and the z mode are coupled to the cavity mode, then the two modes of the two nanoparticles can also be cooled into their ground states. In addition, we find that there exists the dark-mode effect when the powers of the two tweezers are identical, and the dark-mode effect will suppress the cooling of the system. By choosing proper parameters to avoid the dark-mode existing condition, then the dark-mode effect can be broken, and the simultaneous ground-state cooling can be achieved.

The rest of the paper is organized as follows. In Sec. II, we introduce the system consisting of two levitated nanoparticles trapped in a Fabry-Pérot cavity, and analytically derive the Hamiltonians. In Sec. III, we investigate the simultaneous ground-state cooling of the x -direction motions of the two particles, which are located at the nodes of the cavity. In Sec. IV, we study the simultaneous ground-state cooling of both the x - and z -direction motions of the two nanoparticles in a general case. Finally, we present some discussions and a brief conclusion in Sec. V. An Appendix is presented to show the detailed derivation for a part of the interaction Hamiltonians.

II. PHYSICAL MODEL AND HAMILTONIANS

We consider a coupled cavity-levitated-nanoparticle system, in which two dielectric nanoparticles trapped by two optical tweezers are coupled to the field modes in a Fabry-Pérot cavity, as shown in Fig. 1. The Fabry-Pérot cavity, with the cavity axis aligning with the x direction, contains two nanoparticles. The two nanoparticles, placed at $\hat{\mathbf{R}}_1 = (\hat{X}_1, \hat{Y}_1, \hat{Z}_1)$ and $\hat{\mathbf{R}}_2 = (\hat{X}_2, \hat{Y}_2, \hat{Z}_2)$, have the radius $a_0 = 90$ nm, density $\rho \approx 2200$ kg/m³, and dielectric constant $\epsilon_r = 2.07$. We assume that the two optical tweezers have electric fields propagating along the z axis, with the corresponding polarizations $\mathbf{e}_{\text{tw}}^{(1)}$ and $\mathbf{e}_{\text{tw}}^{(2)}$ along the y direction. The foci of the two optical tweezers are located at the positions $(x_{10}, 0, 0)$ and $(x_{20}, 0, 0)$, separated by a distance D . The frequencies of the two optical tweezers are $\omega_{\text{tw}} = 2\pi c/\lambda_{\text{tw}}$, where c is the speed of light in a vacuum and λ_{tw} is the wavelength of the tweezers.

The total Hamiltonian of the system can be written as

$$\hat{H}_{\text{tot}} = \hat{H}_{\text{np}} + \hat{H}_{\text{cav}} + \hat{H}_{\text{int}}. \quad (1)$$

Here, the Hamiltonian \hat{H}_{np} describes the kinetic energy of the center-of-mass motion for the two nanoparticles, and it takes the form

$$\hat{H}_{\text{np}} = \sum_{j=1,2} \frac{\hat{\mathbf{p}}_j^2}{2m}, \quad (2)$$

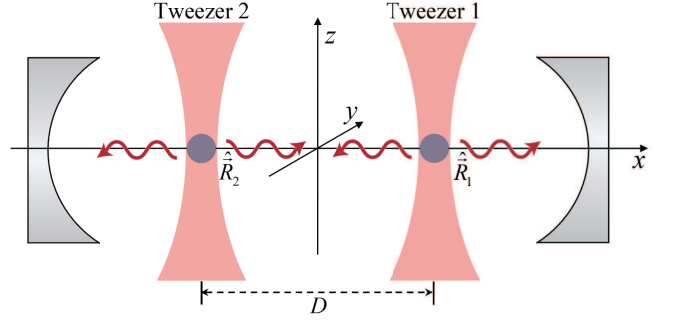


FIG. 1. Schematic of the physical setup. Two dielectric nanoparticles are trapped at positions $\hat{\mathbf{R}}_1$ and $\hat{\mathbf{R}}_2$ by two optical tweezers, where the cavity axis is along the x direction, and the two optical tweezers propagate along the z axis with polarization along the y direction. The distance between the foci of the two tweezers is D .

where $\hat{\mathbf{P}}_j = (\hat{P}_{jx}, \hat{P}_{jy}, \hat{P}_{jz})$ is the three-dimensional momentum operator for the j th ($j = 1, 2$) nanoparticle with mass m . The second term on the right-hand side of Eq. (1) reads

$$\begin{aligned} \hat{H}_{\text{cav}} &= \frac{1}{2} \int [\epsilon_0 \mathbf{E}_{\text{cav}}^2(\mathbf{r}) + \mathbf{B}_{\text{cav}}^2(\mathbf{r}) / \mu_0] d\mathbf{r} \\ &= \sum_j \hbar \omega_j (\hat{a}_j^\dagger \hat{a}_j + 1/2), \end{aligned} \quad (3)$$

where \mathbf{E}_{cav} and \mathbf{B}_{cav} are, respectively, the electric and magnetic fields in the cavity, and ϵ_0 (μ_0) is the free space permittivity (permeability). In addition, ω_j is the resonance frequency of the j th cavity mode (described by the creation and annihilation operators \hat{a}_j^\dagger and \hat{a}_j) in the optical cavity. Since the frequency of the center-of-mass motion for the nanoparticles is much smaller than the free spectrum range of the cavity, we could consider that the two nanoparticles are coupled to a single cavity field mode. Then, the Hamiltonian of the optical cavity can be approximately denoted as $\hat{H}_{\text{cav}} \approx \hbar \omega_{\text{cav}} \hat{a}^\dagger \hat{a}$, where ω_{cav} is the resonance frequency of the cavity mode under consideration with the wave number k , described by the creation and annihilation operators \hat{a}^\dagger and \hat{a} . Note that the zero-point fluctuation term $\hbar \omega_{\text{cav}}/2$ has been omitted in the Hamiltonian.

The last term \hat{H}_{int} in Eq. (1) describes the interactions between the nanoparticles and the electromagnetic fields. In the Rayleigh regime, the radius of the nanoparticle is much smaller than the optical wavelength ($a_0 \ll \lambda$), and the interaction Hamiltonian between the nanoparticles and the electric fields can be written as [48–50]

$$\hat{H}_{\text{int}} \approx -\frac{1}{2} \sum_{j=1,2} \alpha \mathbf{E}^2(\hat{\mathbf{R}}_j), \quad (4)$$

where $\alpha = \epsilon_0 \epsilon_c V$ is the particle polarizability with $\epsilon_c = 3(\epsilon_r - 1)/(\epsilon_r + 2)$ and V being the volume of the nanoparticle. In Eq. (4), $\mathbf{E}(\hat{\mathbf{R}}_j)$ represents the electric field at the position of the j th particle, where $\hat{\mathbf{R}}_j = \mathbf{r}_{j0} + \hat{\mathbf{r}}_j$ denotes the center-of-mass position operator of the j th particle, with $\mathbf{r}_{j0} = (x_{j0}, 0, 0)$ being the focus of the j th optical tweezer along the cavity axis and $\hat{\mathbf{r}}_j = (\hat{x}_j, \hat{y}_j, \hat{z}_j)$ the position operator of the j th particle.

A. The initial electric field

In general, the total electric field at the position $\mathbf{r} = (x, y, z)$ can be approximately written as a sum of the cavity field $\hat{\mathbf{E}}_{\text{cav}}$ and the fields $\mathcal{E}_{\text{tw}}^{(j)}$ for the two optical tweezers,

$$\hat{\mathbf{E}}_I(\mathbf{r}) = \hat{\mathbf{E}}_{\text{cav}}(\mathbf{r}) + \sum_{j=1,2} \mathcal{E}_{\text{tw}}^{(j)}(\mathbf{r}). \quad (5)$$

The first term on the right-hand side of Eq. (5) describes the single-mode electric field of the cavity, which is given by

$$\hat{\mathbf{E}}_{\text{cav}}(\mathbf{r}) = \epsilon_{\text{cav}} \cos(kx - \phi) (\hat{a}^\dagger + \hat{a}) \mathbf{e}_{\text{cav}}, \quad (6)$$

where $\epsilon_{\text{cav}} = \sqrt{\hbar\omega_{\text{cav}}/(2\epsilon_0 V_{\text{cav}})}$ is the amplitude at the center of the cavity with V_{cav} being the cavity volume. For simplicity, we consider the case $\phi = 0$ and the y -axis polarized cavity mode in this paper.

We assume that the two tweezers are sufficiently spaced apart such that the influence of the electric field $\mathcal{E}_{\text{tw}1}$ of the tweezer 1 on the distant nanoparticle 2 can be neglected, and vice versa. Then the total electric fields at the positions of the two nanoparticles 1 and 2 can be approximated as

$$\hat{\mathbf{E}}_I^{(1)}(\hat{\mathbf{R}}_1) = \mathcal{E}_{\text{tw}1}(\hat{\mathbf{R}}_1) + \hat{\mathbf{E}}_{\text{cav}}(\hat{\mathbf{R}}_1), \quad (7a)$$

$$\hat{\mathbf{E}}_I^{(2)}(\hat{\mathbf{R}}_2) = \mathcal{E}_{\text{tw}2}(\hat{\mathbf{R}}_2) + \hat{\mathbf{E}}_{\text{cav}}(\hat{\mathbf{R}}_2). \quad (7b)$$

Typically, the fields of the optical tweezers are considered in coherent states and thus they can be well described by classical fields. Then the electric field of the j th optical tweezer can be expressed by $\mathcal{E}_{\text{tw}j}(\mathbf{r}, t) = \text{Re}[E_{\text{tw}j}(\mathbf{r}, t)]$, where

$$E_{\text{tw}j}(\mathbf{r}, t) = E_{j0}(\mathbf{r}) e^{-i[k_{\text{tw}j}z + \phi_t(\mathbf{r})]} e^{-i\omega_{\text{tw}j}t} \mathbf{e}_{\text{tw}}^{(j)}, \quad (8)$$

with the laser frequency $\omega_{\text{tw}} = ck_{\text{tw}}$ and wave number $k_{\text{tw}} = 2\pi/\lambda_{\text{tw}}$ of the tweezer. We assume that the propagating directions of the two beams are parallel, and that the polarizations $\mathbf{e}_{\text{tw}}^{(1)}$ and $\mathbf{e}_{\text{tw}}^{(2)}$ of the electric fields are along the y direction. Then the real amplitude $E_{j0}(\mathbf{r})$ in Eq. (8) can be written as

$$E_{j0}(\mathbf{r}) = \epsilon_{\text{tw}}^{(j)} \frac{1}{\sqrt{1 + (z/z_R)^2}} \exp\left(-\frac{(x - x_{j0})^2 + y^2}{W^2(z)}\right), \quad (9)$$

where $\epsilon_{\text{tw}}^{(j)} = \sqrt{4P_{\text{tw}}^{(j)}/(\pi\epsilon_0 c W_t^2)}$ is the amplitude of the electric field, with $P_{\text{tw}}^{(j)}$ being the power of the j th laser and W_t the tweezer waist at the focus. In addition, $z_R = \pi W_t^2/\lambda$ is the Rayleigh range and $W(z) = W_t \sqrt{1 + (z/z_R)^2}$. Note that the phase factor $\phi_t(\mathbf{r}) \approx \arctan(z/z_R) - k_{\text{tw}j}z[(x - x_{j0})^2 + y^2]/(2z^2 + 2z_R^2)$ in Eq. (8) can be neglected, since the Rayleigh range z_R is typically several orders of magnitude larger than other length scales. It should be pointed out that, for realistic cases, the phase difference between the two tweezers is a crucial manipulation means, which can be used to control the couplings between the two particles. In this work, we consider a simple case by choosing a zero phase difference, which has been implemented in experiments [77]. For a non-zero phase difference, a direct coupling between the x -direction and z -direction motional modes will be induced, and hence it will make the coupling configuration complicated.

B. The radiation fields

In the Rayleigh regime, the nanoparticle embedded in the electric fields will possess an electric dipole moment, which will create electromagnetic radiation by charge oscillation. Physically, the frequency of the radiation field is equal to that of the incident field. Below, we derive the relation between the radiation field and the dipole. For simplicity in the derivation of the general relation, we use \mathbf{r}_1 and \mathbf{r}_2 (different from $\hat{\mathbf{r}}_j$ introduced before) to denote the positions of the considered point and the dipole, respectively. The electric field at position \mathbf{r}_1 generated by the oscillating dipole at the position \mathbf{r}_2 is given by

$$\mathbf{E}_{\text{rad}}(\mathbf{r}_1) = \overleftrightarrow{\mathbf{G}}(\mathbf{r}_1 - \mathbf{r}_2) \cdot \mathbf{P}(\mathbf{r}_2), \quad (10)$$

where the field propagator (also know as the dyadic Green's function) between the two dipoles is given by [76, 78, 79]

$$\overleftrightarrow{\mathbf{G}}(\mathbf{r}_1 - \mathbf{r}_2) = \frac{e^{ik_0 r_0}}{4\pi\epsilon_0 r_0} \left[\left(\frac{1 - ik_0 r_0}{r_0^2} \right) \frac{3\mathbf{r}_0 \mathbf{r}_0 - r_0^2}{r_0^2} + k_0^2 \frac{r_0^2 - \mathbf{r}_0 \mathbf{r}_0}{r_0^2} \right]. \quad (11)$$

In Eq. (11), k_0 is the wave number of the incident field, $r_0 = |\mathbf{r}_0| = |\mathbf{r}_1 - \mathbf{r}_2|$ is the distance between the two dipoles. Based on Eq. (11), we have the relation $\overleftrightarrow{\mathbf{G}}(\mathbf{r}_1 - \mathbf{r}_2) = \overleftrightarrow{\mathbf{G}}(\mathbf{r}_2 - \mathbf{r}_1) = \overleftrightarrow{\mathbf{G}}(\mathbf{r}_0)$, which can be used to describe the fields related to the two particles. In addition, $\mathbf{r}_0 \mathbf{r}_0 = \sum_{Q Q'} Q_0 Q'_0 \mathbf{e}_Q \mathbf{e}_{Q'}$ with \mathbf{e}_Q being the unit vector in the Q direction and $Q, Q' = x, y, z$. In the following analyses, the Green function can be divided into two parts: $\alpha \overleftrightarrow{\mathbf{G}}(\mathbf{r}_0) = e^{ik_0 r_0} [\eta_n (D/r_0)^3 (1 - ik_0 r_0) \overleftrightarrow{\mathbf{M}}_n(\mathbf{r}_0) + \eta_f (D/r_0) \overleftrightarrow{\mathbf{M}}_f(\mathbf{r}_0)]$ [80], where $\eta_n = 1/4\pi\epsilon_0 D^3$ is the near-field constant and $\eta_f = k_0^2/4\pi\epsilon_0 D$ is the far-field constant. The near-field constant η_n is much smaller than the far-field constant η_f in the far-field regime $k_0 r_0 \gg 1$. In addition, we introduce the near-field tensor

$$\overleftrightarrow{\mathbf{M}}_n(\mathbf{r}) = \frac{1}{r^2} [(3x^2 - r^2)\mathbf{e}_x \mathbf{e}_x + 3xy\mathbf{e}_x \mathbf{e}_y + 3xz\mathbf{e}_x \mathbf{e}_z + 3xy\mathbf{e}_y \mathbf{e}_x + (3y^2 - r^2)\mathbf{e}_y \mathbf{e}_y + 3yz\mathbf{e}_y \mathbf{e}_z + 3xz\mathbf{e}_z \mathbf{e}_x + 3yz\mathbf{e}_z \mathbf{e}_y + (3z^2 - r^2)\mathbf{e}_z \mathbf{e}_z], \quad (12)$$

and the far-field tensor

$$\overleftrightarrow{\mathbf{M}}_f(\mathbf{r}) = \frac{1}{r^2} [(r^2 - x^2)\mathbf{e}_x \mathbf{e}_x - xy\mathbf{e}_x \mathbf{e}_y - xz\mathbf{e}_x \mathbf{e}_z - xy\mathbf{e}_y \mathbf{e}_x + (r^2 - y^2)\mathbf{e}_y \mathbf{e}_y - yz\mathbf{e}_y \mathbf{e}_z - xz\mathbf{e}_z \mathbf{e}_x - yz\mathbf{e}_z \mathbf{e}_y + (r^2 - z^2)\mathbf{e}_z \mathbf{e}_z]. \quad (13)$$

For our considered coupled cavity-levitated-particle system, the total electric field for the j th ($j = 1, 2$) particle is given by the sum of the incident field $\mathbf{E}_I^{(j)}$ and the field emitted by the other dipole,

$$\mathbf{E}_{\text{tot}}^{(j)}(\hat{\mathbf{R}}_j) = \mathbf{E}_I^{(j)}(\hat{\mathbf{R}}_j) + \overleftrightarrow{\mathbf{G}}(\hat{\mathbf{R}}_0) \cdot \mathbf{P}^{(j)}(\hat{\mathbf{R}}_j). \quad (14)$$

Here, $\hat{\mathbf{R}}_0 = \hat{\mathbf{R}}_1 - \hat{\mathbf{R}}_2 = (\hat{X}_0, \hat{Y}_0, \hat{Z}_0)$ and $\mathbf{P}^{(\bar{j})}(\hat{\mathbf{R}}_{\bar{j}}) = \alpha \mathbf{E}_{\text{tot}}^{(\bar{j})}(\hat{\mathbf{R}}_{\bar{j}})$ is the dipole moment generated by the \bar{j} th dielectric nanoparticle, where the index \bar{j} denotes the other particle with respect to the j th particle (namely $\bar{1} = 2$ and $\bar{2} = 1$). Since the cavity field and the tweezer field have different wave numbers, the Green function will take two distinct forms, $\overleftrightarrow{\mathbf{G}}_{\text{cav}}$ and $\overleftrightarrow{\mathbf{G}}_{\text{tw}}$, corresponding to the wave numbers of the cavity field and the tweezer field, respectively. Consequently, the electric field $\mathbf{E}_{\text{tot}}^{(j)}(\hat{\mathbf{R}}_j)$ can be divided into two parts, $\hat{\mathbf{E}}_{\text{tot}}^{(j)}(\hat{\mathbf{R}}_j) = \mathbf{E}_{\text{tot,tw}}^{(j)}(\hat{\mathbf{R}}_j) + \mathbf{E}_{\text{tot,cav}}^{(j)}(\hat{\mathbf{R}}_j)$, with

$$\mathbf{E}_{\text{tot,tw}}^{(j)}(\hat{\mathbf{R}}_j) \approx \mathbf{E}_{\text{tw},j}(\hat{\mathbf{R}}_j, t) + \overleftrightarrow{\mathbf{G}}_{\text{tw}}(\hat{\mathbf{R}}_0) \cdot \alpha \mathbf{E}_{\text{tot,tw}}^{(\bar{j})}(\hat{\mathbf{R}}_{\bar{j}}), \quad (15a)$$

$$\hat{\mathbf{E}}_{\text{tot,cav}}^{(j)}(\hat{\mathbf{R}}_j) \approx \hat{\mathbf{E}}_{\text{cav}}(\hat{\mathbf{R}}_j) + \overleftrightarrow{\mathbf{G}}_{\text{cav}}(\hat{\mathbf{R}}_0) \cdot \alpha \hat{\mathbf{E}}_{\text{tot,cav}}^{(\bar{j})}(\hat{\mathbf{R}}_{\bar{j}}). \quad (15b)$$

Since the magnitude of $\alpha \overleftrightarrow{\mathbf{G}}$ is considerably small compared to the trapping fields, we can neglect the second-order terms in Eqs. (15). Then we obtain the total electric field consisting of the incident field [the tweezer field $\mathcal{E}_{\text{tw}}(\hat{\mathbf{R}}, t)$ and the cavity field $\hat{\mathbf{E}}_{\text{cav}}(\hat{\mathbf{R}})$] and the emitted field [$\mathcal{E}_{\text{Gtw}}(\hat{\mathbf{R}})$ and $\hat{\mathcal{E}}_{\text{Gcav}}(\hat{\mathbf{R}})$] by the dipole,

$$\begin{aligned} \hat{\mathcal{E}}_{\text{tot}}^{(j)}(\hat{\mathbf{R}}_j) &= \mathcal{E}_{\text{tw},j}(\hat{\mathbf{R}}_j, t) + \hat{\mathbf{E}}_{\text{cav}}(\hat{\mathbf{R}}_j) \\ &\quad + \mathcal{E}_{\text{Gtw},\bar{j}}(\hat{\mathbf{R}}_j) + \hat{\mathcal{E}}_{\text{Gcav}}(\hat{\mathbf{R}}_j), \end{aligned} \quad (16)$$

where $\mathcal{E}_{\text{Gtw},\bar{j}}(\hat{\mathbf{R}}_j) = \text{Re}[\overleftrightarrow{\mathbf{G}}_{\text{tw}}(\hat{\mathbf{R}}_0) \cdot \alpha \mathbf{E}_{\text{tw},\bar{j}}(\hat{\mathbf{R}}_{\bar{j}}, t)]$ describes the radiation field generated by the oscillating dipoles at $\hat{\mathbf{R}}_{\bar{j}}$, which is induced by the \bar{j} th tweezer field $\mathbf{E}_{\text{tw},\bar{j}}(\hat{\mathbf{R}}_{\bar{j}})$. In addition, $\hat{\mathcal{E}}_{\text{Gcav}}(\hat{\mathbf{R}}_j) = \text{Re}[\overleftrightarrow{\mathbf{G}}_{\text{cav}}(\hat{\mathbf{R}}_0) \cdot \alpha \hat{\mathbf{E}}_{\text{cav}}(\hat{\mathbf{R}}_{\bar{j}})]$ represents the radiation field produced by the dipole moment, which is induced by the cavity field at the position $\hat{\mathbf{R}}_{\bar{j}}$.

C. The interaction Hamiltonians

In this section, we present the detailed expressions of the interaction Hamiltonians by putting the electric field operator $\mathcal{E}_{\text{tot}}^{(j)}(\hat{\mathbf{R}}_j, t)$ given by Eq. (16) into Hamiltonian (4). The interaction Hamiltonian can be divided into two parts $\hat{H}_{\text{int}} = \sum_{j=1,2} \hat{H}_{\text{int}}^{(j)}$, where the forms of the two parts are similar. Below, we take the j th (for $j=1,2$) particle as an example. The Hamiltonian $\hat{H}_{\text{int}}^{(j)}$ can be written as

$$\begin{aligned} \hat{H}_{\text{int}}^{(j)} &= -\frac{1}{2} \alpha [\mathcal{E}_{\text{tw},j}(\hat{\mathbf{R}}_j, t) + \hat{\mathbf{E}}_{\text{cav}}(\hat{\mathbf{R}}_j) \\ &\quad + \mathcal{E}_{\text{Gtw},\bar{j}}(\hat{\mathbf{R}}_j) + \hat{\mathcal{E}}_{\text{Gcav}}(\hat{\mathbf{R}}_j)]^2, \end{aligned} \quad (17)$$

which can be further divided into six terms

$$\begin{aligned} \hat{H}_{\text{int}}^{(j)} &= \hat{H}_{\text{cs}}^{(j)} + \hat{H}_{\text{rad-rad}}^{(j)} + \hat{H}_{\text{tw-Gtw}}^{(j)} \\ &\quad + \hat{H}_{\text{cav-Gcav}}^{(j)} + \hat{H}_{\text{tw-Gcav}}^{(j)} + \hat{H}_{\text{cav-Gtw}}^{(j)}, \end{aligned} \quad (18)$$

each of which represents a special physical interaction.

The first term $\hat{H}_{\text{cs}}^{(j)}$ in Eq. (18) is the standard interaction Hamiltonian of the cavity-field with the j th levitated particle

$$\hat{H}_{\text{cs}}^{(j)} = -\frac{1}{2} \alpha [\mathcal{E}_{\text{tw},j}(\hat{\mathbf{R}}_j, t) + \hat{\mathbf{E}}_{\text{cav}}(\hat{\mathbf{R}}_j)]^2, \quad (19)$$

which consists of three parts $\hat{H}_{\text{cs}}^{(j)} = \hat{H}_{\text{tw-tw}}^{(j)} + \hat{H}_{\text{cav-cav}}^{(j)} + \hat{H}_{\text{cav-tw}}^{(j)}$. Since the j th particle is trapped near the focus of the tweezer, we can approximate the electric field of the tweezer by its expansion near $\mathbf{r}_{j0} = (x_{j0}, 0, 0)$. Then, we can obtain the harmonic potential energy of the tweezer as $\hat{H}_{\text{tw-tw}}^{(j)} = -\alpha \mathcal{E}_{\text{tw},j}^2(\hat{\mathbf{R}}_j)/2 \approx \sum_Q m \omega_{jQ}^2 \hat{Q}_j^2/2$ with $Q = x, y, z$, where we employ the rotating-wave approximation and neglect both the $\exp(\pm 2i\omega_{\text{tw}}t)$ terms and the constant terms. This means that the j th nanoparticle is trapped by the tweezer with trapping frequencies $[\omega_{jx}, \omega_{jy}, \omega_{jz}] = \sqrt{\alpha/2m} \epsilon_{\text{tw}}^{(j)} [\sqrt{2}W_t^{-1}, \sqrt{2}W_t^{-1}, z_R^{-1}]$. The square term of the cavity field contains both the cavity frequency shift and the radiation pressure effect, $\hat{H}_{\text{cav-cav}}^{(j)} = -\alpha \hat{\mathbf{E}}_{\text{cav}}^2(\hat{\mathbf{R}}_j)/2 \approx \hbar \omega_{\text{sh}} \hat{a}^\dagger \hat{a} + \hbar g_{ax} \hat{a}^\dagger \hat{a} \hat{x}_j$, where $\omega_{\text{sh}} = -\alpha \epsilon_{\text{cav}}^2 \cos^2(kx_{j0})/\hbar$ and $g_{ax} = \alpha \epsilon_{\text{cav}}^2 2 \cos(kx_{j0}) \sin(kx_{j0})k/\hbar$. In addition, the interaction term between the tweezer and cavity fields is given by $\hat{H}_{\text{tw-cav}}^{(j)} = -\alpha [\mathcal{E}_{\text{tw},j}(\hat{\mathbf{R}}_j) \cdot \hat{\mathbf{E}}_{\text{cav}}(\hat{\mathbf{R}}_j)] \approx \hbar \Omega (\hat{a}^\dagger + \hat{a}) + \hbar g_{xj} (\hat{a}^\dagger + \hat{a}) \hat{x}_j + i \hbar g_{zj} (\hat{a} - \hat{a}^\dagger) \hat{z}_j$, which describes the displacement of the cavity mode and the coupling mediated by coherent scattering, where $\Omega = -\alpha \epsilon_{\text{cav}} \epsilon_{\text{tw}}^{(j)} \cos(kx_{j0})/(2\hbar)$, $g_{xj} = \alpha \epsilon_{\text{cav}} \epsilon_{\text{tw}}^{(j)} \sin(kx_{j0})k/(2\hbar)$, and $g_{zj} = -\alpha \epsilon_{\text{cav}} \epsilon_{\text{tw}}^{(j)} \cos(kx_{j0})k_{\text{tw}}/(2\hbar)$ [48–50].

The second term $\hat{H}_{\text{rad-rad}}^{(j)}$ in Eq. (18) describes the interaction between these radiation fields at position $\hat{\mathbf{R}}_j$ generated by the \bar{j} th oscillating dipole, and it is written as

$$\hat{H}_{\text{rad-rad}}^{(j)} = -\frac{1}{2} \alpha [\mathcal{E}_{\text{Gtw},\bar{j}}(\hat{\mathbf{R}}_j) + \hat{\mathcal{E}}_{\text{Gcav}}(\hat{\mathbf{R}}_j)]^2. \quad (20)$$

We point out that the terms $\hat{H}_{\text{rad-rad}}^{(j)}$ for $j = 1, 2$ are higher-order term of α compared to the other terms, so the terms are usually small enough to be ignored.

The remaining terms in Eq. (18) describe the interactions between the incident field at the position of j th particle and the field at position $\hat{\mathbf{R}}_j$ generated by the \bar{j} th dipole. Concretely, these interaction Hamiltonians are given by

$$\hat{H}_{\text{tw-Gtw}}^{(j)} = -\alpha \mathcal{E}_{\text{tw},j}(\hat{\mathbf{R}}_j, t) \cdot \mathcal{E}_{\text{Gtw},\bar{j}}(\hat{\mathbf{R}}_j), \quad (21a)$$

$$\hat{H}_{\text{cav-Gcav}}^{(j)} = -\alpha \hat{\mathbf{E}}_{\text{cav}}(\hat{\mathbf{R}}_j) \cdot \hat{\mathcal{E}}_{\text{Gcav}}(\hat{\mathbf{R}}_j), \quad (21b)$$

$$\hat{H}_{\text{tw-Gcav}}^{(j)} = -\alpha \mathcal{E}_{\text{tw},j}(\hat{\mathbf{R}}_j, t) \cdot \hat{\mathcal{E}}_{\text{Gcav}}(\hat{\mathbf{R}}_j), \quad (21c)$$

$$\hat{H}_{\text{cav-Gtw}}^{(j)} = -\alpha \hat{\mathbf{E}}_{\text{cav}}(\hat{\mathbf{R}}_j) \cdot \mathcal{E}_{\text{Gtw},\bar{j}}(\hat{\mathbf{R}}_j). \quad (21d)$$

The four cross terms describe the interactions between the incident field and the radiation field, and they are generated by the mechanical effect of scattered light via the optical binding force. Equations (21a) and (21b) describe the lateral binding and longitudinal binding, respectively. The optical binding force can be calculated as [76, 77]

$$\mathbf{F}^{\text{bind}} = \frac{1}{2} \nabla \text{Re} \left[\mathbf{P}^*(\mathbf{R}_j) \cdot \overleftrightarrow{\mathbf{G}}(\mathbf{R}_j - \mathbf{R}_i) \cdot \alpha \mathbf{E}(\mathbf{R}_i) \right], \quad (22)$$

where the force term describes the interaction between the emitted field and the dipole at \mathbf{R}_j . Equation (21a) describes the interaction corresponding to the case where the two particles are placed on the x -axis, and they are trapped by the two optical tweezers with the same frequency, respectively. Here,

the two tweezers polarize along the y -axis. In this case, the binding force acting on particle 1 has the following components:

$$F_x^{(1)} = \frac{\alpha^2 E_{10} E_{20}}{8\pi\epsilon_0 R_0^4} [3 \cos(k_{\text{tw}} R_0) + 3k_{\text{tw}} R_0 \sin(k_{\text{tw}} R_0) - 2(k_{\text{tw}} R_0)^2 \cos(k_{\text{tw}} R_0) - (k_{\text{tw}} R_0)^3 \sin(k_{\text{tw}} R_0)], \quad (23a)$$

$$F_y^{(1)} = 0, \quad (23b)$$

$$F_z^{(1)} = \frac{\alpha^2 E_{10} E_{20}}{8\pi\epsilon_0 R_0^4} [-k_{\text{tw}} R_0 \sin(k_{\text{tw}} R_0) + (k_{\text{tw}} R_0)^2 \cos(k_{\text{tw}} R_0) + (k_{\text{tw}} R_0)^3 \sin(k_{\text{tw}} R_0)], \quad (23c)$$

along the x , y , and z axes, respectively, with the distance R_0 between the two particles.

The Green function $\vec{\mathbf{G}}(r_0)$ [Eq. (11)] contains these terms proportional to r_0^{-1} , r_0^{-2} , and r_0^{-3} . In the far-field region $k_0 r_0 \gg 1$, the terms with r_0^{-1} dominate in the case, and then the Green function retains only the last term, i.e., $\alpha \vec{\mathbf{G}}(r_0) \approx e^{ik_0 r_0} \eta_f(D/r_0) \vec{\mathbf{M}}_f(r_0)$. To investigate the specific scope of the far-field region, we compare in Fig. 2 the optical binding forces corresponding to the exact calculation and the far-field approximation. As shown in Fig. 2, we can find that the forces experience oscillations, and that as the scaled displacement increases, the oscillation amplitudes of the optical binding forces decrease. This oscillation behavior can be understood because the forces are functions of the trigonometric functions, as shown in Eqs. (23). Meanwhile, it can be seen from Fig. 2 that the exact optical-binding force is very close to the approximate optical-binding force when $R_0/\lambda > 1$, which is consistent with the fact that the near-field constant is much smaller than the far-field constant when $R_0 \sim \lambda$.

Since these interaction terms described by Eqs. (21) involve two particles, below we analyze these cross interactions between the two particles together in the far-field regime. The first cross term $\hat{H}_{\text{tw-Gtw}} = \hat{H}_{\text{tw-Gtw}}^{(1)} + \hat{H}_{\text{tw-Gtw}}^{(2)}$ describes the lateral binding of the two identical spherical nanoparticles. It is given by

$$\begin{aligned} \hat{H}_{\text{tw-Gtw}} &\approx -\frac{1}{2} \alpha \eta_{f_{\text{tw}}}(D/\hat{R}_0) E_{10}(\hat{\mathbf{R}}_1) E_{20}(\hat{\mathbf{R}}_2) \\ &\times \left\{ \cos[k_{\text{tw}}(\hat{\mathbf{Z}}_0 + \hat{\mathbf{R}}_0)] \mathbf{e}_{\text{tw}}^{(1)} \cdot \vec{\mathbf{M}}_f(\hat{\mathbf{R}}_0) \cdot \mathbf{e}_{\text{tw}}^{(2)} \right. \\ &\left. + \cos[k_{\text{tw}}(\hat{\mathbf{Z}}_0 - \hat{\mathbf{R}}_0)] \mathbf{e}_{\text{tw}}^{(2)} \cdot \vec{\mathbf{M}}_f(\hat{\mathbf{R}}_0) \cdot \mathbf{e}_{\text{tw}}^{(1)} \right\}, \quad (24) \end{aligned}$$

where $\eta_{f_{\text{tw}}}$ corresponds to the far-field constant for the wave number k_{tw} . The detailed derivation can be found in the Appendix. Expanding the corresponding electric field near the foci of tweezers 1 and 2, the $\hat{H}_{\text{tw-Gtw}}$ can be rewritten as

$$\begin{aligned} \hat{H}_{\text{tw-Gtw}} &\approx \hbar R_\alpha (\hat{x}_1 - \hat{x}_2) \\ &+ \sum_{q=x,y,z} \left[v_q (\hat{q}_1^2 + \hat{q}_2^2) + \frac{1}{2} k_q (\hat{q}_1 - \hat{q}_2)^2 \right], \quad (25) \end{aligned}$$

where the first term corresponds to a shift of the equilibrium position of the center-of-mass motion along x -axis, and the

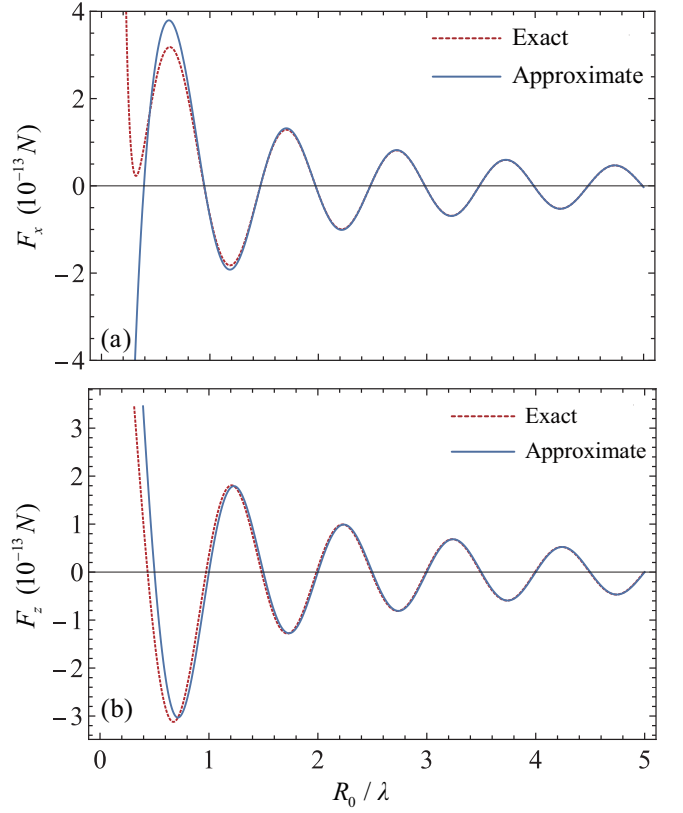


FIG. 2. Comparison of the exact and approximate results concerning the optical binding forces (a) F_x and (b) F_z (along the x axis and z axis) between the two nanoparticles as functions of the scaled distance R_0/λ . The radius of the two nanoparticles is $a_0 = 90$ nm, the numerical apertures of the two tweezers are $\text{NA} \approx 0.8$, and the powers of the two tweezers are $P_{\text{tw}}^{(1)} = 0.8$ W and $P_{\text{tw}}^{(2)} = 0.45$ W.

displacement factor is given by

$$R_\alpha = \alpha \eta_{f_{\text{tw}}} \epsilon_{\text{tw}}^{(1)} \epsilon_{\text{tw}}^{(2)} [k_{\text{tw}} \sin(k_{\text{tw}} D) + D^{-1} \cos(k_{\text{tw}} D)] / \hbar. \quad (26)$$

The second term in Eq. (25) describes the frequency shifts of the center-of-mass motion, with the frequency shifts

$$v_x = v_y = \alpha \eta_{f_{\text{tw}}} \epsilon_{\text{tw}}^{(1)} \epsilon_{\text{tw}}^{(2)} \cos(k_{\text{tw}} D) / W_t^2, \quad (27a)$$

$$v_z = \alpha \eta_{f_{\text{tw}}} \epsilon_{\text{tw}}^{(1)} \epsilon_{\text{tw}}^{(2)} \cos(k_{\text{tw}} D) / (2z_R^2). \quad (27b)$$

The third term in Eq. (25) describes the interaction between the two particles mediated by the light scattering, and the particle-particle coupling strengths are given by

$$k_x = -\alpha \eta_{f_{\text{tw}}} \epsilon_{\text{tw}}^{(1)} \epsilon_{\text{tw}}^{(2)} [(2D^{-2} - k_{\text{tw}}^2) \cos(k_{\text{tw}} D) + 2k_{\text{tw}} D^{-1} \sin(k_{\text{tw}} D)], \quad (28a)$$

$$k_y = \alpha \eta_{f_{\text{tw}}} \epsilon_{\text{tw}}^{(1)} \epsilon_{\text{tw}}^{(2)} [3D^{-2} \cos(k_{\text{tw}} D) + k_{\text{tw}} D^{-1} \sin(k_{\text{tw}} D)], \quad (28b)$$

$$k_z = \alpha \eta_{f_{\text{tw}}} \epsilon_{\text{tw}}^{(1)} \epsilon_{\text{tw}}^{(2)} [(D^{-2} + k_{\text{tw}}^2) \cos(k_{\text{tw}} D) + k_{\text{tw}} D^{-1} \sin(k_{\text{tw}} D)]. \quad (28c)$$

The second cross term $\hat{H}_{\text{cav-Gcav}}$ given by Eq. (21b) represents the longitudinal binding of the two spherical nanoparticles,

$$\begin{aligned}\hat{H}_{\text{cav-Gcav}} &= \hat{H}_{\text{cav-Gcav}}^{(1)} + \hat{H}_{\text{cav-Gcav}}^{(2)} \\ &\approx -4\alpha\eta_f\epsilon_{\text{cav}}^2(D/\hat{R}_0)\cos(k\hat{X}_1)\cos(k\hat{X}_2) \\ &\quad \times \cos(k\hat{R}_0)(\hat{a}^\dagger\hat{a} + 1/2)\mathbf{e}_{\text{cav}} \cdot \overleftrightarrow{\mathbf{M}}_f(\hat{\mathbf{R}}_0) \cdot \mathbf{e}_{\text{cav}}\end{aligned}\quad (29)$$

where η_f corresponds to the far-field constant for the wave number k . The Hamiltonian $\hat{H}_{\text{cav-Gcav}}$ can be further re-expressed as

$$\begin{aligned}\hat{H}_{\text{cav-Gcav}} &\approx -4\alpha\eta_f\epsilon_{\text{cav}}^2\cos(kx_{10})\cos(kx_{20})\cos(kD)\hat{a}^\dagger\hat{a} \\ &\quad + \hbar g_\alpha \hat{x}_1(\hat{a}^\dagger\hat{a} + 1/2) - \hbar g_\alpha \hat{x}_2(\hat{a}^\dagger\hat{a} + 1/2),\end{aligned}\quad (30)$$

where the first term is the frequency shift term and the last two terms are the optomechanical coupling terms, with the coupling strength

$$\begin{aligned}g_\alpha &= 4\alpha\eta_f\epsilon_{\text{cav}}^2[(k\sin(kD) + D^{-1}\cos(kD)) \\ &\quad \times \cos^2(kD/2) + k\sin(kD)\cos(kD)/2]/\hbar.\end{aligned}\quad (31)$$

The third cross term $\hat{H}_{\text{tw-Gcav}}$ describes the interaction between the j th tweezer field at $\hat{\mathbf{R}}_j$ and the field generated by the other dipole caused by the cavity field. This term reads

$$\begin{aligned}\hat{H}_{\text{tw-Gcav}} &= \hat{H}_{\text{tw-Gcav}}^{(1)} + \hat{H}_{\text{tw-Gcav}}^{(2)} \\ &\approx -\frac{1}{2}\alpha\eta_f\epsilon_{\text{cav}}(D/\hat{R}_0)\cos(k\hat{R}_0)E_{10}(\hat{\mathbf{R}}_1)\cos(k\hat{X}_2) \\ &\quad \times (\hat{a}^\dagger e^{-ik_{\text{tw}}\hat{Z}_1} + \hat{a}e^{ik_{\text{tw}}\hat{Z}_1})\mathbf{e}_{\text{tw}}^{(1)} \cdot \overleftrightarrow{\mathbf{M}}_f(\hat{\mathbf{R}}_0) \cdot \mathbf{e}_{\text{cav}} \\ &\quad - \frac{1}{2}\alpha\epsilon_{\text{cav}}\eta_f(D/\hat{R}_0)\cos(k\hat{R}_0)E_{20}(\hat{\mathbf{R}}_2)\cos(k\hat{X}_1) \\ &\quad \times (\hat{a}^\dagger e^{-ik_{\text{tw}}\hat{Z}_2} + \hat{a}e^{ik_{\text{tw}}\hat{Z}_2})\mathbf{e}_{\text{tw}}^{(2)} \cdot \overleftrightarrow{\mathbf{M}}_f(\hat{\mathbf{R}}_0) \cdot \mathbf{e}_{\text{cav}},\end{aligned}\quad (32)$$

which can be rewritten as

$$\begin{aligned}\hat{H}_{\text{tw-Gcav}} &\approx \hbar\Omega_\alpha(\hat{a}^\dagger + \hat{a}) + \sum_{j=1,2}\hbar g_{\alpha x_j}(\hat{a}^\dagger + \hat{a})\hat{x}_j \\ &\quad + \sum_{j=1,2}i\hbar g_{\alpha z_j}(\hat{a} - \hat{a}^\dagger)\hat{z}_j.\end{aligned}\quad (33)$$

In Eq. (33), we introduced $\Omega_\alpha = -\alpha\eta_f\epsilon_{\text{cav}}\cos(kD)\cos(kD/2)(\epsilon_{\text{tw}}^{(1)} + \epsilon_{\text{tw}}^{(2)})/(2\hbar)$ and the coupling strengths

$$\begin{aligned}g_{\alpha x_1} &= \frac{1}{2\hbar}\alpha\eta_f\epsilon_{\text{cav}}[(k\sin(kD) + D^{-1}\cos(kD))(\epsilon_{\text{tw}}^{(1)} + \epsilon_{\text{tw}}^{(2)}) \\ &\quad \times \cos(kD/2) + k\cos(kD)\epsilon_{\text{tw}}^{(2)}\sin(kD/2)],\end{aligned}\quad (34a)$$

$$\begin{aligned}g_{\alpha x_2} &= -\frac{1}{2\hbar}\alpha\eta_f\epsilon_{\text{cav}}[(k\sin(kD) + D^{-1}\cos(kD))(\epsilon_{\text{tw}}^{(1)} + \epsilon_{\text{tw}}^{(2)}) \\ &\quad \times \cos(kD/2) + k\cos(kD)\epsilon_{\text{tw}}^{(1)}\sin(kD/2)],\end{aligned}\quad (34b)$$

$$g_{\alpha z_j} = \frac{1}{2\hbar}\alpha\eta_f\epsilon_{\text{cav}}\epsilon_{\text{tw}}^{(j)}k_{\text{tw}}\cos(kD)\cos(kD/2).\quad (34c)$$

Finally, the interaction Hamiltonian between the cavity field and the field emitted by the dipole induced by the tweezer fields reads

$$\begin{aligned}\hat{H}_{\text{cav-Gtw}} &= \hat{H}_{\text{cav-Gtw}}^{(1)} + \hat{H}_{\text{cav-Gtw}}^{(2)} \\ &\approx -\frac{1}{2}\alpha\eta_{f_{\text{tw}}}\epsilon_{\text{cav}}(D/\hat{R}_0)\cos(k\hat{X}_1)E_{20}(\hat{\mathbf{R}}_2)(\hat{a}e^{-ik_{\text{tw}}(\hat{R}_0-\hat{Z}_2)} \\ &\quad + \hat{a}^\dagger e^{ik_{\text{tw}}(\hat{R}_0-\hat{Z}_2)})\mathbf{e}_{\text{cav}} \cdot \overleftrightarrow{\mathbf{M}}_f(\hat{\mathbf{R}}_0) \cdot \mathbf{e}_{\text{tw}}^{(2)} \\ &\quad - \frac{1}{2}\alpha\epsilon_{\text{cav}}\eta_{f_{\text{tw}}}(D/\hat{R}_0)\cos(k\hat{X}_2)E_{10}(\hat{\mathbf{R}}_1)(\hat{a}e^{-ik_{\text{tw}}(\hat{R}_0-\hat{Z}_1)} \\ &\quad + \hat{a}^\dagger e^{ik_{\text{tw}}(\hat{R}_0-\hat{Z}_1)})\mathbf{e}_{\text{cav}} \cdot \overleftrightarrow{\mathbf{M}}_f(\hat{\mathbf{R}}_0) \cdot \mathbf{e}_{\text{tw}}^{(1)},\end{aligned}\quad (35)$$

which can be further expressed as

$$\begin{aligned}\hat{H}_{\text{cav-Gtw}} &\approx \hbar(\Omega_\beta\hat{a} + \Omega_\beta^*\hat{a}^\dagger) + \sum_{j=1,2}\hbar(g_{\beta x_j}\hat{a} + g_{\beta x_j}^*\hat{a}^\dagger)\hat{x}_j \\ &\quad + \sum_{j=1,2}i\hbar(g_{\beta z_j}\hat{a} - g_{\beta z_j}^*\hat{a}^\dagger)\hat{z}_j.\end{aligned}\quad (36)$$

Here, the displacement factor of mode a is $\Omega_\beta = -\alpha\eta_{f_{\text{tw}}}\epsilon_{\text{cav}}(\epsilon_{\text{tw}}^{(1)} + \epsilon_{\text{tw}}^{(2)})\cos(kD/2)e^{-ik_{\text{tw}}D}/(2\hbar)$ and the coupling strengths are

$$\begin{aligned}g_{\beta x_1} &= \frac{1}{2\hbar}\alpha\eta_{f_{\text{tw}}}\epsilon_{\text{cav}}[(D^{-1} + ik_{\text{tw}})(\epsilon_{\text{tw}}^{(1)} + \epsilon_{\text{tw}}^{(2)}) \\ &\quad \times \cos(kD/2) + \epsilon_{\text{tw}}^{(2)}k\sin(kD/2)]e^{-ik_{\text{tw}}D},\end{aligned}\quad (37a)$$

$$\begin{aligned}g_{\beta x_2} &= -\frac{1}{2\hbar}\alpha\eta_{f_{\text{tw}}}\epsilon_{\text{cav}}[(D^{-1} + ik_{\text{tw}})(\epsilon_{\text{tw}}^{(1)} + \epsilon_{\text{tw}}^{(2)}) \\ &\quad \times \cos(kD/2) + \epsilon_{\text{tw}}^{(1)}k\sin(kD/2)]e^{-ik_{\text{tw}}D},\end{aligned}\quad (37b)$$

$$g_{\beta z_j} = -\frac{1}{2\hbar}\alpha\eta_{f_{\text{tw}}}\epsilon_{\text{cav}}\epsilon_{\text{tw}}^{(j)}k_{\text{tw}}\cos(kD/2)e^{-ik_{\text{tw}}D}.\quad (37c)$$

Based on the above analyses, we obtain the total Hamiltonian in the rotating frame [defined by the unitary transformation operator $\exp(-i\omega_{\text{tw}}\hat{a}^\dagger\hat{a}t)$] as

$$\begin{aligned}\hat{H}_{\text{tot}} &= \hbar\Delta'\hat{a}^\dagger\hat{a} + \sum_{j=1,2}\frac{\hat{\mathbf{p}}_j^2}{2m} + \sum_{j=1,2}\sum_{Q=x,y,z}\frac{1}{2}m_j\tilde{\omega}_{jQ}^2\hat{Q}_j^2 \\ &\quad + \sum_{j=1,2}\hbar\tilde{g}_{\alpha x_j}\hat{a}^\dagger\hat{a}\hat{x}_j - \sum_{Q=x,y,z}k_Q\hat{Q}_1\hat{Q}_2 \\ &\quad + \hbar(\tilde{\Omega}\hat{a} + \tilde{\Omega}^*\hat{a}^\dagger) + \hbar\tilde{R}(\hat{x}_1 - \hat{x}_2) \\ &\quad + \hbar\sum_{j=1,2}[\hat{a}(\tilde{g}_{x_j}\hat{x}_j + i\tilde{g}_{z_j}\hat{z}_j) + \text{H.c.}],\end{aligned}\quad (38)$$

where the effective driving detuning is $\Delta' = \Delta - 2\alpha\epsilon_{\text{cav}}^2\cos^2(kD/2)/\hbar - 4\alpha\epsilon_{\text{cav}}^2\eta_f\cos^2(kD/2)\cos(kD)/\hbar$ with $\Delta = \omega_{\text{cav}} - \omega_{\text{tw}}$. The j th particle exhibits a Q -mode frequency of $\tilde{\omega}_{jQ} = \sqrt{\omega_{jQ}^2 + 2\nu_Q/m + k_Q/m}$ with $j = 1, 2$ and $Q = x, y, z$, the displacement factor of the cavity mode and x modes are, respectively, given by $\tilde{\Omega} = \Omega + \Omega_\alpha + \Omega_\beta$ and $\tilde{R}_j = R_\alpha + g_\alpha/2$, and the optomechanical couplings are given by $\tilde{g}_{\alpha x_j} = g_{\alpha x_j} - (-1)^j g_\alpha$ and $\tilde{g}_{x(z)_j} = g_{x(z)_j} + g_{\alpha x(z)_j} + g_{\beta x(z)_j}$. It can be seen from Eq. (38) that the y modes of the two particles are only coupled to each other and decoupled from the

other modes, so we will only consider the x and z modes in the following discussions. It should be pointed out that if the polarization direction of the two optical tweezers is not perpendicular to the cavity axis, the coupling channel between the y modes and the other modes will be turned on. We also note that, to be concise, the hat for all the operators will be ignored in the following.

III. SIMULTANEOUS GROUND-STATE COOLING OF THE X-DIRECTION MOTIONS

For cooling of the x -direction (along the cavity axis) motion of a single-levitated nanoparticle, we prefer to locate the particle at the nodes of the cavity mode $|\sin(kx_0)| = 1$ [48]. Below we consider that the two particles are located at $x_{10} = D/2$ and $x_{20} = -D/2$, which satisfy $\sin(kx_{10}) = 1$ and $\sin(kx_{20}) = -1$. To cool the mechanical modes, we consider the red-sideband resonance regime: $\Delta = \omega_{\text{cav}} - \omega_{\text{tw}} = \omega_{\text{m}}$. Concretely, we assume that the tweezer laser has the wavelength $\lambda_{\text{tw}} = 1064$ nm and the trapping frequency of the particles is $\omega_{\text{m}}/2\pi \sim 100$ MHz. Therefore, the driving frequency is much larger than the resonance frequency of the oscillator $\omega_{\text{tw}} \gg \omega_{\text{m}}$, then the wave number of the cavity field is approximately equal to that of the tweezer field $k \approx k_{\text{tw}}$, and we can make the following approximations: $\sin(k_{\text{tw}}D/2) \approx 1$, $\cos(k_{\text{tw}}D/2) \approx 0$, $\cos(kD) \approx \cos(k_{\text{tw}}D) \approx -1$, $\sin(kD) \approx \cos(k_{\text{tw}}D) \approx 0$, and $e^{-ik_{\text{tw}}D} \approx e^{ik_{\text{tw}}D} \approx -1$. In this case, the z modes of the two particles are decoupled from other modes (x modes and the cavity mode a). The z modes of the two particles are coupled to each other via the z - z coupling, and the z -mode motion cannot be cooled because they are connected with the environments and decoupled from the cooling channel. For studying the cooling of mechanical motion, in this section we focus on the x modes and cavity mode. In this case, the Hamiltonian of the system including the x modes and cavity mode is reduced to

$$H_{\text{tot}} = \hbar\Delta a^\dagger a + \sum_{j=1,2} \left(\frac{P_{jx}^2}{2m} + \frac{m\Omega_j^2 x_j^2}{2} \right) + \hbar R(x_1 - x_2) + \sum_{j=1,2} \hbar g_j (a^\dagger + a)x_j - k_x x_1 x_2, \quad (39)$$

where the x -mode oscillation frequency of the j th nanoparticle is given by $\Omega_j^2 = (\alpha_{\text{tw}}^{(j)2}/W_t^2 - 2\alpha\eta_{f_{\text{tw}}}\epsilon_{\text{tw}}^{(1)}\epsilon_{\text{tw}}^{(2)}/W_t^2 + k_x)/m$, the coupling strengths are given by

$$g_1 = \alpha\epsilon_{\text{cav}}[\epsilon_{\text{tw}}^{(1)} - (\eta_f + \eta_{f_{\text{tw}}})\epsilon_{\text{tw}}^{(2)}]k/(2\hbar), \quad (40a)$$

$$g_2 = -\alpha\epsilon_{\text{cav}}[\epsilon_{\text{tw}}^{(2)} - (\eta_f + \eta_{f_{\text{tw}}})\epsilon_{\text{tw}}^{(1)}]k/(2\hbar), \quad (40b)$$

and the displacement factor is

$$R = -\alpha\eta_{f_{\text{tw}}}\epsilon_{\text{tw}}^{(1)}\epsilon_{\text{tw}}^{(2)}/(\hbar D). \quad (41)$$

We see from Hamiltonian (39) that there exist bilinear couplings between the cavity field and the x -direction motions. In addition, the two harmonic oscillations are coupled with each other via the x - x interaction, and both the two oscillators are

displaced in the x -direction. For analyzing the cooling of the x -direction motion, below we will work in the displaced representation of the system such that the excitations are associated with the fluctuations. For convenience, we introduce the dimensionless position and momentum operators $\sqrt{2}q_{j=1,2} = x_j/x_{j,\text{zpf}}$ and $\sqrt{2}p_{j=1,2} = P_{jx}/p_{j,\text{zpf}}$, where the zero-point motions are $x_{j,\text{zpf}} = \sqrt{\hbar/(2m\Omega_j)}$ and $p_{j,\text{zpf}} = \sqrt{m\Omega_j\hbar/2}$. We also introduce the quadrature operators $X = (a^\dagger + a)/\sqrt{2}$ and $Y = i(a^\dagger - a)/\sqrt{2}$ for the cavity field.

Based on Eq. (39), we can obtain the quantum Langevin equations for the system as

$$\dot{q}_1 = \Omega_1 p_1, \quad (42a)$$

$$\dot{p}_1 = -\Omega_1 q_1 - \sqrt{2}G_1 X - R_1 + G_x q_2 - \gamma_1 p_1 + f_{\text{th}}^{(1)}, \quad (42b)$$

$$\dot{q}_2 = \Omega_2 p_2, \quad (42c)$$

$$\dot{p}_2 = -\Omega_2 q_2 - \sqrt{2}G_2 X + R_2 + G_x q_1 - \gamma_2 p_2 + f_{\text{th}}^{(2)}, \quad (42d)$$

$$\dot{X} = \Delta Y - \kappa X + \sqrt{2}\kappa X_{\text{in}}, \quad (42e)$$

$$\dot{Y} = -\Delta X - \kappa Y - \sqrt{2} \sum_{j=1,2} G_j q_j + \sqrt{2}\kappa Y_{\text{in}}, \quad (42f)$$

where κ and γ_j are the decay rates of the cavity mode and the x -direction motion of the j th particle, respectively. In Eqs. (42), we introduce $G_j = \sqrt{2}g_j x_{j,\text{zpf}}$, $G_x = 2k_x x_{1,\text{zpf}} x_{2,\text{zpf}}/\hbar$, and $R_j = \sqrt{2}R x_{j,\text{zpf}}$. The $f_{\text{th}}^{(j)}$ is the stochastic thermal noise operator corresponding to the x -mode motion of the j th particle, which is determined by the zero average values

$$\langle f_{\text{th}}^{(j)}(t) \rangle = 0, \quad j = 1, 2, \quad (43)$$

and the correlation function,

$$\langle f_{\text{th}}^{(j)}(t) f_{\text{th}}^{(j')}(t') \rangle = \delta_{jj'} \frac{\gamma_j}{\Omega_j} \int e^{-i\omega(t-t')}\omega \left[\coth\left(\frac{\hbar\omega}{2k_B T_j}\right) + 1 \right] \frac{d\omega}{2\pi}, \quad (44)$$

where k_B is the Boltzmann constant, and T_j is the temperature of the thermal bath associated with the x_j mode. We assume that these mechanical modes are connected to the high-temperature reservoirs ($k_B T_j \gg \hbar\Omega_j$), so we can obtain $\coth[\hbar\Omega_j/(k_B T_j)] + 1 \approx 2k_B T_j/(\hbar\Omega_j)$ in the high-temperature limit. The stochastic noise is reduced to a delta-correlation noise $\langle f_{\text{th}}^{(j)}(t) f_{\text{th}}^{(j')}(t') + f_{\text{th}}^{(j')}(t') f_{\text{th}}^{(j)}(t) \rangle \approx 2\gamma_j(2\bar{n}_{j,\text{th}} + 1)\delta(t-t')\delta_{jj'}$, where $\bar{n}_{j,\text{th}} = [\exp[\hbar\Omega_j/(k_B T_j)] - 1]^{-1} \approx k_B T_j/(\hbar\Omega_j)$ is the thermal occupation number for the j th thermal bath. In addition, the $X_{\text{in}} = (a_{\text{in}}^\dagger + a_{\text{in}})/\sqrt{2}$ and $Y_{\text{in}} = i(a_{\text{in}}^\dagger - a_{\text{in}})/\sqrt{2}$ are the optical noise operators, which are determined by the zero average values $\langle X_{\text{in}} \rangle = 0$ and $\langle Y_{\text{in}} \rangle = 0$. The correlation functions of these optical noise operators are

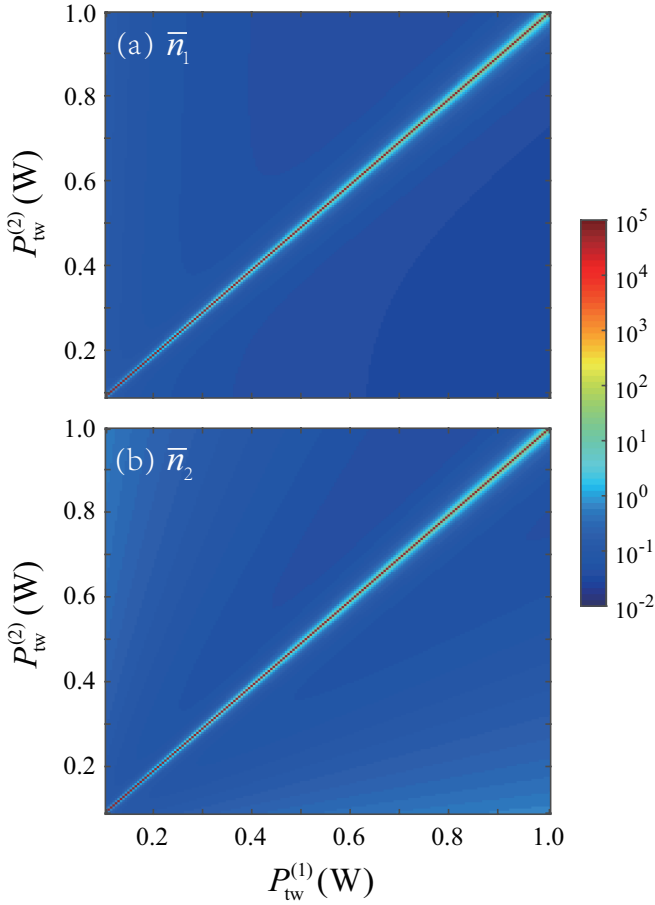


FIG. 3. The final mean phonon numbers (a) \bar{n}_1 and (b) \bar{n}_2 in the two mechanical modes versus the powers $P_{\text{tw}}^{(1)}$ and $P_{\text{tw}}^{(2)}$ of the two tweezers. The silica nanoparticle of radius is $a_0 \approx 90$ nm, the separation of the particles is $D \approx 2.5\lambda$, the initial occupations are $\bar{n}_{1,\text{th}} = \bar{n}_{2,\text{th}} = 10^5$, and the effective driving detuning is $\Delta = \Omega_1$. Other parameters used are $\gamma_1/\Omega_1 = \gamma_2/\Omega_1 = 0.5 \times 10^{-8}$ and $\kappa/\Omega_1 = 0.2$.

given by [81]

$$\langle X_{\text{in}}(t) X_{\text{in}}(t') \rangle = \frac{1}{2} \delta(t - t'), \quad (45a)$$

$$\langle Y_{\text{in}}(t) Y_{\text{in}}(t') \rangle = \frac{1}{2} \delta(t - t'), \quad (45b)$$

$$\langle X_{\text{in}}(t) Y_{\text{in}}(t') \rangle = \frac{i}{2} \delta(t - t'), \quad (45c)$$

$$\langle Y_{\text{in}}(t) X_{\text{in}}(t') \rangle = -\frac{i}{2} \delta(t - t'). \quad (45d)$$

To work in the displacement representation, we re-express Eqs. (42a)–(42f) around the steady-state values by writing operators $O \in \{q_{j=1,2}, p_{j=1,2}, X, Y\}$ as the sum of average value and quantum fluctuation: $O = \langle O \rangle + \delta O$. Then, the Langevin equations can be separated into the semi-classical equations of motion and the equations of motion for quantum fluctuations.

The latter can be written as

$$\delta \dot{q}_1 = \Omega_1 \delta p_1, \quad (46a)$$

$$\delta \dot{p}_1 = -\Omega_1 \delta q_1 - \sqrt{2} G_1 \delta X + G_x \delta q_2 - \gamma_1 \delta p_1 + f_{\text{th}}^{(1)}, \quad (46b)$$

$$\delta \dot{q}_2 = \Omega_2 \delta p_2, \quad (46c)$$

$$\delta \dot{p}_2 = -\Omega_2 \delta q_2 - \sqrt{2} G_2 \delta X + G_x \delta q_1 - \gamma_2 \delta p_2 + f_{\text{th}}^{(2)}, \quad (46d)$$

$$\delta \dot{X} = \Delta \delta Y - \kappa \delta X + \sqrt{2\kappa} \delta X_{\text{in}}, \quad (46e)$$

$$\delta \dot{Y} = -\Delta \delta X - \kappa \delta Y - \sum_{j=1,2} \sqrt{2} G_j \delta q_j + \sqrt{2\kappa} \delta Y_{\text{in}}. \quad (46f)$$

By introducing the operator vector

$$\mathbf{u}(t) = (\delta q_1, \delta p_1, \delta q_2, \delta p_2, \delta X, \delta Y)^T, \quad (47)$$

with “T” denotes the matrix transpose, and the noise operator vector

$$\mathbf{N}(t) = (0, f_{\text{th}}^{(1)}(t), 0, f_{\text{th}}^{(2)}(t), \sqrt{2\kappa} \delta X_{\text{in}}(t), \sqrt{2\kappa} \delta Y_{\text{in}}(t))^T, \quad (48)$$

Eqs. (46) can be expressed as a compact matrix form

$$\dot{\mathbf{u}}(t) = \mathbf{A} \mathbf{u}(t) + \mathbf{N}(t), \quad (49)$$

where the coefficient matrix \mathbf{A} is given by

$$\mathbf{A} = \begin{pmatrix} 0 & \Omega_1 & 0 & 0 & 0 & 0 \\ -\Omega_1 & -\gamma_1 & G_x & 0 & -\sqrt{2} G_1 & 0 \\ 0 & 0 & 0 & \Omega_2 & 0 & 0 \\ G_x & 0 & -\Omega_2 & -\gamma_2 & -\sqrt{2} G_2 & 0 \\ 0 & 0 & 0 & 0 & -\kappa & \Delta \\ -\sqrt{2} G_1 & 0 & -\sqrt{2} G_2 & 0 & -\Delta & -\kappa \end{pmatrix}. \quad (50)$$

To calculate the final mean phonon numbers in these mechanical modes, we introduce the covariance matrix \mathbf{V} defined by the matrix elements

$$\mathbf{V}_{nm} = \frac{1}{2} [\mathbf{u}_n(\infty) \mathbf{u}_m(\infty) + \mathbf{u}_m(\infty) \mathbf{u}_n(\infty)] \quad (51)$$

for $n, m = 1-6$. The covariance matrix \mathbf{V} is determined by the Lyapunov equation [82]

$$\mathbf{A} \mathbf{V} + \mathbf{V} \mathbf{A}^T = -\mathbf{Q}, \quad (52)$$

where \mathbf{Q} is the noise correlation matrix, defined by the elements $\mathbf{Q}_{nm} = \frac{1}{2} \langle \mathbf{N}_n(t) \mathbf{N}_m(t') + \mathbf{N}_m(t) \mathbf{N}_n(t') \rangle$ for $n, m = 1-6$. Based on Eqs. (44) and (45), the noise correlation matrix can be obtained as

$$\mathbf{Q} = \text{diag} [0, \gamma_1 (2\bar{n}_{1,\text{th}} + 1), 0, \gamma_2 (2\bar{n}_{2,\text{th}} + 1), \kappa, \kappa]. \quad (53)$$

The final mean phonon numbers of the two mechanical modes can be expressed as

$$\bar{n}_j = \frac{1}{2} [\langle \delta q_j^2 \rangle + \langle \delta p_j^2 \rangle - 1], \quad j = 1, 2, \quad (54)$$

where the stationary variance of the mechanical modes is given by the corresponding diagonal matrix elements of the covariance matrix,

$$\langle \delta q_1^2 \rangle = \mathbf{V}_{11}, \quad \langle \delta p_1^2 \rangle = \mathbf{V}_{22}, \quad (55a)$$

$$\langle \delta q_2^2 \rangle = \mathbf{V}_{33}, \quad \langle \delta p_2^2 \rangle = \mathbf{V}_{44}. \quad (55b)$$

Therefore, the final mean phonon numbers in the two mechanical modes can be obtained by solving the Lyapunov equation. Note that the stability conditions for the steady states in our simulations have been confirmed with the Routh-Hurwitz criterion [83].

In the coupled cavity-levitated-nanoparticles system, the powers of the optical tweezers affect both the resonance frequencies of the mechanical modes and the coupling strengths between the cavity mode and the mechanical modes. Below, we analyze the dependence of the cooling efficiency of the x modes of the two nanoparticles on the powers of the two optical tweezers. In Fig. 3, we plot the final mean phonon numbers \bar{n}_1 and \bar{n}_2 as functions of the powers $P_{\text{tw}}^{(1)}$ and $P_{\text{tw}}^{(2)}$. We can see from Fig. 3 that the cooling of the two modes x_1 and x_2 is strongly suppressed when the two tweezers have the same power. The cooling performance becomes better when the working point deviates the diagonal line $P_{\text{tw}}^{(1)} = P_{\text{tw}}^{(2)}$. This phenomenon can be well explained based on the dark-mode effect [51, 84–90]. From the expressions of Ω_j and G_j , we know that, when the powers of the two optical tweezers are equal, i.e., $P_{\text{tw}}^{(1)} = P_{\text{tw}}^{(2)}$, the two modes x_1 and x_2 have the same resonance frequency $\Omega_1 = \Omega_2$, and the optomechanical coupling strengths are equal but with opposite signs $G_1 = -G_2$. In the following, we analyze the dark-mode effect in the system under these parameters.

Using the dimensionless operators, the Hamiltonian characterizing the quantum fluctuations can be written as

$$H_{\text{lin}}/\hbar = \Delta a^\dagger a + \sum_{j=1,2} \left[\frac{\Omega_j}{2} (p_j^2 + q_j^2) + G_j (a^\dagger + a) q_j \right] - G_x q_1 q_2. \quad (56)$$

To clearly see the dark-mode effect in the system, we define two hybrid modes of the two mechanical modes as

$$q_+ = \frac{G_1 q_1 + G_2 q_2}{\sqrt{G_1^2 + G_2^2}}, \quad p_+ = \frac{G_1 p_1 + G_2 p_2}{\sqrt{G_1^2 + G_2^2}}, \quad (57a)$$

$$q_- = \frac{G_1 q_2 - G_2 q_1}{\sqrt{G_1^2 + G_2^2}}, \quad p_- = \frac{G_1 p_2 - G_2 p_1}{\sqrt{G_1^2 + G_2^2}}. \quad (57b)$$

In the representation of the two new hybrid modes, the Hamiltonian H_{lin} can be expressed as

$$\begin{aligned} H_{\text{lin}}/\hbar = & \Delta a^\dagger a + \frac{\Omega_+}{2} (q_+^2 + p_+^2) + \frac{\Omega_-}{2} (q_-^2 + p_-^2) \\ & + G_q q_+ q_- + G_p p_+ p_- + G_+(a^\dagger + a) q_+ \\ & - G_x \frac{G_1 G_2 q_+^2 - G_1 G_2 q_-^2}{G_1^2 + G_2^2}, \end{aligned} \quad (58)$$

where the resonance frequencies of the two hybrid modes are introduced by

$$\Omega_+ = \frac{\Omega_1 G_1^2 + \Omega_2 G_2^2}{G_1^2 + G_2^2}, \quad \Omega_- = \frac{\Omega_1 G_2^2 + \Omega_2 G_1^2}{G_1^2 + G_2^2}. \quad (59)$$

In addition, the optomechanical coupling strength between the cavity mode a and the hybrid mode q_+ is given by $G_+ =$

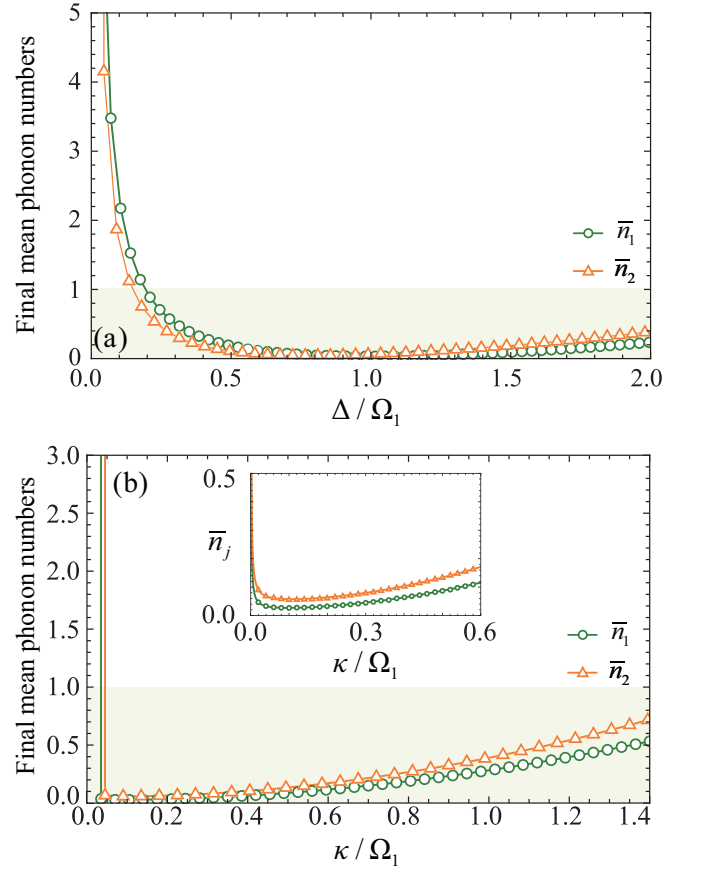


FIG. 4. (a) The final mean phonon numbers \bar{n}_1 (green solid line with circles) and \bar{n}_2 (yellow solid line with triangles) versus the scaled driving detuning Δ/Ω_1 when $\kappa/\Omega_1 = 0.2$. (b) The final average phonon numbers \bar{n}_1 and \bar{n}_2 versus the scaled cavity linewidth κ/Ω_1 at $\Delta/\Omega_1 = 1$. The inset is a zoom-in plot of the phonon numbers in a narrower range of κ/Ω_1 . Other common parameters used are $P_{\text{tw}}^{(1)} = 0.8$ W, $P_{\text{tw}}^{(2)} = 0.45$ W, $\bar{n}_{1,\text{th}} = \bar{n}_{2,\text{th}} = 10^5$, $\Omega_2/\Omega_1 \approx 0.75$, $G_1/\Omega_1 \approx 0.22$, $G_2/\Omega_1 \approx -0.19$, $G_x/\Omega_1 \approx -0.046$, and $\gamma_1/\Omega_1 = \gamma_2/\Omega_1 = 0.5 \times 10^{-8}$.

$\sqrt{G_1^2 + G_2^2}$, and the other two coupling strengths between the two modes q_{\pm} are given by

$$G_q = \frac{(\Omega_2 - \Omega_1) G_1 G_2 - k_x (G_1^2 - G_2^2)}{G_1^2 + G_2^2}, \quad (60a)$$

$$G_p = \frac{(\Omega_2 - \Omega_1) G_1 G_2}{G_1^2 + G_2^2}. \quad (60b)$$

It can be seen from Eq. (58) that, when $\Omega_1 = \Omega_2$ and $G_1 = -G_2$, we have $G_q = G_p = 0$, and thus the mode q_- is decoupled from both the mode q_+ and the cavity mode a . In this case, the mode q_- becomes a dark mode, and it cannot be cooled via the cavity-field cooling channel. In order to realize the simultaneous ground-state cooling of the two modes q_1 and q_2 , we need to take different optical tweezers powers, i.e., $P_{\text{tw}}^{(1)} \neq P_{\text{tw}}^{(2)}$, then the dark-mode effect is broken.

In Fig. 4(a), we plot the final mean phonon numbers \bar{n}_1 and \bar{n}_2 for the two mechanical modes as functions of the scaled

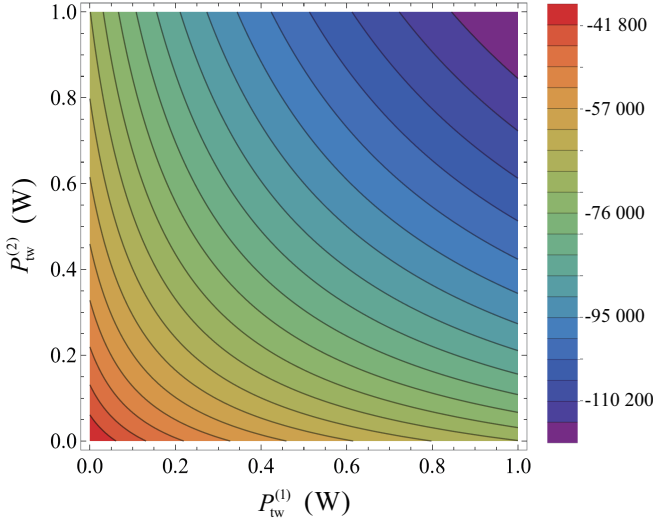


FIG. 5. The particle-particle coupling strength G_x versus the powers $P_{\text{tw}}^{(1)}$ and $P_{\text{tw}}^{(2)}$ of the two optical tweezers. Here, we take the following parameters: the radius of the two silica nanoparticles $a_0 \approx 90$ nm, the wavelength $\lambda = 1064$ nm, and the numerical aperture $\text{NA} \approx 0.8$.

detuning Δ/Ω_1 in the nondegenerate-mechanical-mode case, $\Omega_2 \approx 0.75\Omega_1$. In this case, we obtain the mechanical frequencies $\Omega_{x,y,z}/2\pi \approx (324, 366, 130)$ kHz for the center-of-mass motion of the particle 1. For this system, the nanoparticle is levitated in a vacuum, and hence it is highly isolated from the environment, resulting in a high Q factor exceeding 10^8 [91]. Under these parameters, the simultaneous ground-state cooling of the two mechanical modes can be realized ($\bar{n}_1, \bar{n}_2 < 1$). In particular, the optimal cooling of the mode x_j for the j th particle appears around the red-sideband resonances: $\Delta/\Omega_j \approx 1$. Note that the slight shifts of the resonance point are caused by the couplings among the optical modes and two mechanical modes. We point out that the present cooling mechanism is essentially a sideband cooling. Therefore, we need to investigate the dependence of the cooling performance on the sideband-resolution condition. To this end, we plot in Fig. 4(b) the final mean phonon numbers \bar{n}_1 and \bar{n}_2 as functions of the scaled cavity-field decay rate κ/Ω_1 . Here we can see that the final mean phonon numbers \bar{n}_1 and \bar{n}_2 firstly decrease and then increase with the increase of the decay rate κ (See the inset) [92, 93].

In this system, there exists a coupling between the two mechanical modes with the coupling strength G_x . Below, we investigate how the coupling strength G_x affects the cooling results of the two mechanical modes. Firstly, we point out that the particle-particle coupling strength used in Fig. 4 is $G_x \approx -0.046\Omega_1$, where the distance between the two particles is given by $D \approx 2.5\lambda$. It can be confirmed from Fig. 2 that the used parameters satisfy the far-field approximation well. In addition, it can be seen from Eq. (28a) that the particle-particle coupling strength G_x can be adjusted by the powers $P_{\text{tw}}^{(1)}$ and $P_{\text{tw}}^{(2)}$ of the two tweezers and the distance D of the two particles. To further elucidate this point, in Fig. 5 we plot the particle-particle coupling strength G_x versus the powers

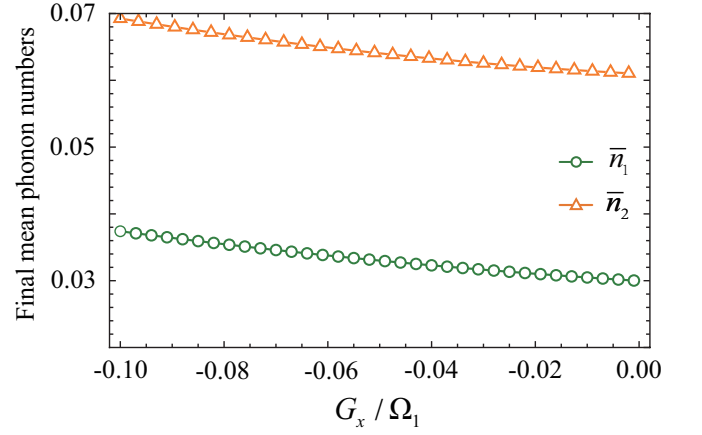


FIG. 6. The final mean phonon numbers \bar{n}_1 (green solid line with circles) and \bar{n}_2 (yellow solid line with triangles) as functions of G_x/Ω_1 when $\Delta = \Omega_1$ and $\kappa/\Omega_1 = 0.2$. Other parameters used are the same as those in Fig. 4

$P_{\text{tw}}^{(1)}$ and $P_{\text{tw}}^{(2)}$ of the two tweezers. Figure 5 exhibits that the strength G_x increases with the increase of the two powers $P_{\text{tw}}^{(1)}$ and $P_{\text{tw}}^{(2)}$, which is consistent with the phenomenon that the optical binding force between the two levitated particles increases with the powers of the two tweezers. Moreover, we find that G_x can be adjusted from -41.8 kHz to -110.2 kHz and the scaled coupling $G_x/\Omega_1 \in [-0.1, -0.03]$. Since the particle-particle coupling provides a channel for the exchange of thermal excitations between the two mechanical modes x_1 and x_2 , it is interesting to analyze the dependence of the cooling results on the coupling strength G_x . In Fig. 6, we plot the final mean phonon numbers \bar{n}_1 and \bar{n}_2 as functions of the scaled particle-particle coupling strength G_x/Ω_1 . Figure 6 shows that both the final mean phonon numbers \bar{n}_1 and \bar{n}_2 of particles 1 and 2 increase with the increase of the absolute value of the particle-particle coupling $|G_x|$, which means that the increase of the $|G_x|$ will reduce the cooling efficiency of the two modes x_1 and x_2 .

We mention that there exists a dilemma in the choosing of the resonance frequencies $\Omega_{j=1,2}$. As shown in Eq. (56), the dipole-induced coupling determines the phonon exchange between the two mechanical modes, and this effect is strong in the resonant case. To break the dark-mode effect, however, we prefer to consider two detuned mechanical modes. In our simulations, we choose detuned mechanical modes such that the dark-mode effect is broken. In this case, the dipole-induced coupling is partly suppressed but it still works.

IV. SIMULTANEOUS COOLING OF X- AND Z-DIRECTION MOTIONS

In Sec. III, we study the special case where the distance between the two particles takes special values, resulting in the decoupling of the cavity mode a from the z -direction motions of the two particles. However, when the distance between the two particles does not take these special positions, the cavity

mode a will couple to the z -direction motions of the two particles. In the following, we will analyze the cooling of both x - and z -direction motions of the two particles in this case.

For a general case, the system is described by the Hamiltonian (38). Here, there exist nonlinear couplings between the cavity mode and the x -direction motions of the two particles. In particular, we consider the case where the driving [the $\tilde{\Omega}$ term in Eq. (38)] of the cavity mode is strong enough, then we can linearize the system and obtain the linearized Langevin equations as

$$\dot{\mathbf{u}}'(t) = \mathbf{A}'\mathbf{u}'(t) + \mathbf{N}'(t). \quad (61)$$

$$\mathbf{A}' = \begin{pmatrix} 0 & \tilde{\omega}_{1x} & 0 & 0 & 0 & 0 & 0 & 0 & 0 & 0 \\ -\tilde{\omega}_{1x} & -\gamma_{1x} & G_x & 0 & 0 & 0 & 0 & 0 & -\sqrt{2}A_1 & \sqrt{2}B_1 \\ 0 & 0 & 0 & \tilde{\omega}_{2x} & 0 & 0 & 0 & 0 & 0 & 0 \\ G_x & 0 & -\tilde{\omega}_{2x} & -\gamma_{2x} & 0 & 0 & 0 & 0 & -\sqrt{2}A_2 & \sqrt{2}B_2 \\ 0 & 0 & 0 & 0 & 0 & \tilde{\omega}_{1z} & 0 & 0 & 0 & 0 \\ 0 & 0 & 0 & 0 & -\tilde{\omega}_{1z} & -\gamma_{1z} & G_z & 0 & -\sqrt{2}C_1 & -\sqrt{2}D_1 \\ 0 & 0 & 0 & 0 & 0 & 0 & 0 & \tilde{\omega}_{2z} & 0 & 0 \\ 0 & 0 & 0 & 0 & G_z & 0 & -\tilde{\omega}_{2z} & -\gamma_{2z} & -\sqrt{2}C_2 & -\sqrt{2}D_2 \\ -\sqrt{2}B_1 & 0 & -\sqrt{2}B_2 & 0 & -\sqrt{2}D_1 & 0 & -\sqrt{2}D_2 & 0 & -\kappa & +\tilde{\Delta} \\ -\sqrt{2}A_1 & 0 & -\sqrt{2}A_2 & 0 & -\sqrt{2}C_1 & 0 & -\sqrt{2}C_2 & 0 & -\tilde{\Delta} & -\kappa \end{pmatrix}. \quad (64)$$

In Eq. (64), we have defined $G_x = 2k_x x_{1,zpf} x_{2,zpf} / \hbar$, $G_z = 2k_z z_{1,zpf} z_{2,zpf} / \hbar$, $G_{x_j} = \sqrt{2} \tilde{g}_{x_j} x_{j,zpf}$, $G_{z_j} = i\sqrt{2} \tilde{g}_{z_j} z_{j,zpf}$, and $G_{ax_j} = \sqrt{2} \tilde{g}_{ax_j} \langle a^\dagger \rangle x_{j,zpf}$, then the linearized optomechanical-coupling strengths are given by $\tilde{G}_{jx} = G_{x_j} + G_{ax_j}$ and $\tilde{G}_{jz} = G_{z_j}$. These complex coupling strengths can be divided into real and imaginary parts, namely, $\tilde{G}_{jx} = A_j + iB_j$ and $\tilde{G}_{jz} = C_j + iD_j$, where A_j , B_j , C_j , and D_j have been introduced in Eq. (64).

These linearized coupling strengths depend on the semi-classical motion, which are governed by the semi-classical equations of motion. In the steady-state case, the average values of the system operators can be obtained as

$$\langle a \rangle = \frac{i\tilde{\Omega}^* + iG_{x_1}^* \langle x_1 \rangle + iG_{x_2}^* \langle x_2 \rangle + iG_{z_1}^* \langle z_1 \rangle + iG_{z_2}^* \langle z_2 \rangle}{-i\tilde{\Delta} - \kappa}, \quad (65a)$$

$$\langle x_1 \rangle = \frac{-G_{ax_1} \langle a \rangle + G_x \langle x_2 \rangle - \tilde{R}_1 - 2\text{Im}[G_{x_1} \langle a \rangle]}{\tilde{\omega}_{1x}}, \quad (65b)$$

$$\langle x_2 \rangle = \frac{-G_{ax_2} \langle a \rangle + G_x \langle x_1 \rangle + \tilde{R}_2 - 2\text{Im}[G_{x_2} \langle a \rangle]}{\tilde{\omega}_{2x}}, \quad (65c)$$

$$\langle z_1 \rangle = \frac{G_z \langle z_2 \rangle - 2\text{Im}[G_{z_1} \langle a \rangle]}{\tilde{\omega}_{1z}}, \quad (65d)$$

$$\langle z_2 \rangle = \frac{G_z \langle z_1 \rangle - 2\text{Im}[G_{z_2} \langle a \rangle]}{\tilde{\omega}_{2z}}, \quad (65e)$$

where $\tilde{\Delta} = \Delta' + \tilde{g}_{ax_1} x_{1,zpf} \langle x_1 \rangle + \tilde{g}_{ax_2} x_{2,zpf} \langle x_2 \rangle$ and $\tilde{R}_j =$

Here the fluctuation operator vector is defined by

$$\mathbf{u}'(t) = (\delta q_{1x}, \delta p_{1x}, \delta q_{2x}, \delta p_{2x}, \delta q_{1z}, \delta p_{1z}, \delta q_{2z}, \delta p_{2z}, \delta X, \delta Y)^T, \quad (62)$$

where the mechanical quadratures are introduced as $\sqrt{2}\delta q_{jx} = x_j/x_{j,zpf}$, $\sqrt{2}\delta p_{jx} = P_{jx}/p_{jx,zpf}$, $\sqrt{2}\delta q_{jz} = z_j/z_{j,zpf}$, and $\sqrt{2}\delta p_{jz} = P_{jz}/p_{jz,zpf}$ with $j = 1, 2$. In Eq. (61), the noise operator vector is defined by

$$\mathbf{N}'(t) = (0, f_{\text{th}}^{(1x)}(t), 0, f_{\text{th}}^{(2x)}(t), 0, f_{\text{th}}^{(1z)}(t), 0, f_{\text{th}}^{(2z)}(t), \sqrt{2\kappa}\delta X_{\text{in}}(t), \sqrt{2\kappa}\delta Y_{\text{in}}(t))^T, \quad (63)$$

and the coefficient matrix is given by

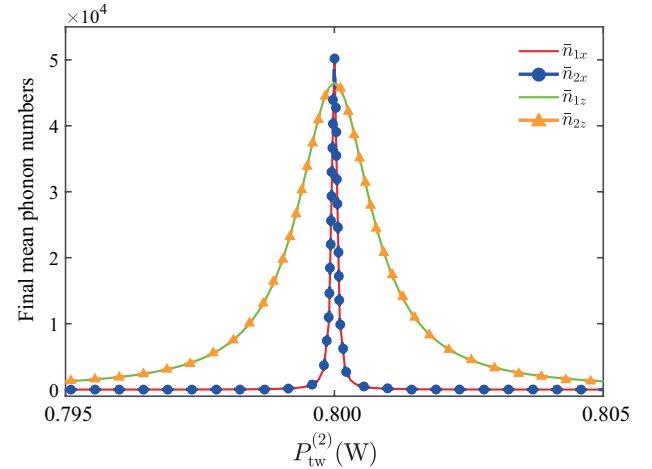


FIG. 7. The final mean phonon numbers \bar{n}_{1x} (red line), \bar{n}_{2x} (blue dashed line with dots), \bar{n}_{1z} (green line), and \bar{n}_{2z} (yellow dashed line with triangles) in the four mechanical modes versus the power $P_{\text{tw}}^{(2)}$ of the tweezer 2. Other parameters used are $P_{\text{tw}}^{(1)} = 0.8$ W, $\bar{n}_{1x,\text{th}} = \bar{n}_{2x,\text{th}} = \bar{n}_{1z,\text{th}} = \bar{n}_{2z,\text{th}} = 10^5$, $\gamma_{1x}/\tilde{\omega}_{1x} = \gamma_{1z}/\tilde{\omega}_{1x} = \gamma_{2x}/\tilde{\omega}_{1x} = \gamma_{2z}/\tilde{\omega}_{1x} = 0.5 \times 10^{-8}$, and $\kappa/\tilde{\omega}_{1x} = 0.2$.

$\sqrt{2}\tilde{R}_{x_j,zpf}$. Based on the linearized Langevin equations, we can derive an effective Hamiltonian to describe the linearized

dynamics of the system as

$$H'_{\text{lin}}/\hbar = \tilde{\Delta}\delta a^\dagger\delta a + \sum_l \left[\frac{\tilde{\omega}_l}{2}(\delta q_l^2 + \delta p_l^2) + (\tilde{G}_l\delta a + \tilde{G}_l^*\delta a^\dagger)\delta q_l \right] - G_x\delta q_{1x}\delta q_{2x} - G_z\delta q_{1z}\delta q_{2z}, \quad (66)$$

where $l = 1x, 2x, 1z, 2z$.

It can be seen from Eq. (66) that, the cavity mode δa is coupled to the four modes δq_{1x} , δq_{1z} , δq_{2x} , and δq_{2z} . Meanwhile, the modes δq_{1x} and δq_{1z} are coupled to the modes δq_{2x} and δq_{2z} , respectively. To investigate the dependence of the cooling performance of the four mechanical modes on the powers of the two tweezers, in Fig. 7, we plot the final mean phonon number \bar{n}_{1x} , \bar{n}_{1z} , \bar{n}_{2x} , and \bar{n}_{2z} as functions of $P_{\text{tw}}^{(2)}$ when $P_{\text{tw}}^{(1)} = 0.8$ W. Here, we can see that all the modes cannot be cooled around the identical power point $P_{\text{tw}}^{(1)} \approx P_{\text{tw}}^{(2)}$. The phenomenon can be explained based on the dark-mode effect. In this five-mode system, when $P_{\text{tw}}^{(1)} = P_{\text{tw}}^{(2)}$, we have $\tilde{\omega}_{1x} = \tilde{\omega}_{2x}$ and $\tilde{\omega}_{1z} = \tilde{\omega}_{2z}$. Meanwhile, the coupling strengths satisfy the relations: $G_{x_1} = -G_{x_2}$, $G_{ax_1} = -G_{ax_2}$, and $G_{z_1} = G_{z_2}$. To analyze the dark-mode effect, we introduce the creation and annihilation operators $b_l^\dagger = (\delta q_l - i\delta p_l)/\sqrt{2}$ and $b_l = (\delta q_l + i\delta p_l)/\sqrt{2}$ of these mechanical modes. We further define four hybrid mechanical modes as

$$B_{1+} = \frac{\tilde{G}_{1x}b_{1x} + \tilde{G}_{2x}b_{2x}}{\sqrt{|\tilde{G}_{1x}|^2 + |\tilde{G}_{2x}|^2}}, \quad B_{1-} = \frac{\tilde{G}_{2x}^*b_{1x} - \tilde{G}_{1x}^*b_{2x}}{\sqrt{|\tilde{G}_{1x}|^2 + |\tilde{G}_{2x}|^2}}, \quad (67a)$$

$$B_{2+} = \frac{\tilde{G}_{1z}b_{1z} + \tilde{G}_{2z}b_{2z}}{\sqrt{|\tilde{G}_{1z}|^2 + |\tilde{G}_{2z}|^2}}, \quad B_{2-} = \frac{\tilde{G}_{2z}^*b_{1z} - \tilde{G}_{1z}^*b_{2z}}{\sqrt{|\tilde{G}_{1z}|^2 + |\tilde{G}_{2z}|^2}}. \quad (67b)$$

In the hybrid-mode representation, the Hamiltonian (66) can be re-expressed as a new form, which is not presented here because of its complicated form. By analyzing the Hamiltonian in the hybrid-mode representation, we find that the dark-mode effect appears under the conditions $\tilde{\omega}_{1x(z)} = \tilde{\omega}_{2x(z)}$ and $\tilde{G}_{1x(z)}^2 = \tilde{G}_{2x(z)}^2$. Accordingly, in the identical power case under consideration, the $x(z)$ modes of the two particles have the same frequency $\tilde{\omega}_{1x(z)} = \tilde{\omega}_{2x(z)}$ and absolute value of coupling strength $|\tilde{G}_{1x(z)}| = |\tilde{G}_{2x(z)}|$, and then the Hamiltonian is reduced to

$$H'_{\text{lin}}/\hbar = \Delta\delta a^\dagger\delta a + \sum_{j=1,2} \tilde{\omega}_j(B_{j+}^\dagger B_{j+} + B_{j-}^\dagger B_{j-}) + \sum_{j=1,2} (-1)^j [(\xi_j B_{j+}^\dagger + \xi_j^* B_{j+})^2 - (\xi_j B_{j-}^\dagger + \xi_j B_{j-})^2] + [\tilde{G}_{1x}(\zeta_1 B_{1+} + \zeta_1^* B_{1+}^\dagger)a + \tilde{G}_{1z}(\zeta_2 B_{2+} + \zeta_2^* B_{2+}^\dagger)a + \text{H.c.}], \quad (68)$$

where we have ignored the constant term. In Eq. (68), the normalized resonance frequencies are $\tilde{\omega}_1 = \tilde{\omega}_{1x}$ and $\tilde{\omega}_2 = \tilde{\omega}_{1z}$, and other parameters used are defined as $\zeta_1 = G_x/2\tilde{G}_{1x}^*$, $\zeta_2 = G_z/2\tilde{G}_{1z}$, $\xi_1 = \sqrt{2}\tilde{G}_{1x}^*/|\tilde{G}_{1x}|$, and $\xi_2 = \sqrt{2}\tilde{G}_{1z}^*/|\tilde{G}_{1z}|$. We can see from Eq. (68) that the two modes B_{1-} and B_{2-} are decoupled from other modes, and hence become the dark

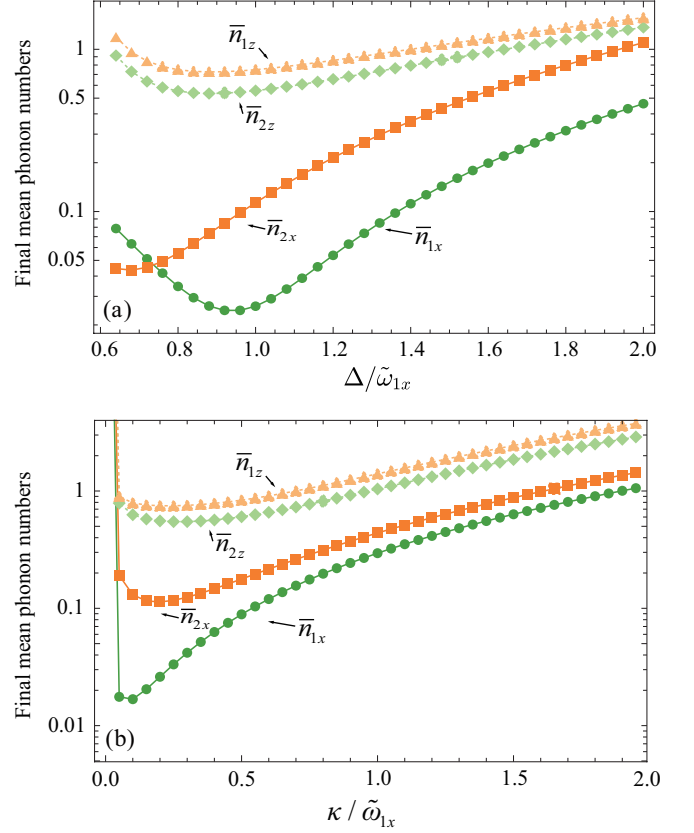


FIG. 8. The final mean phonon numbers \bar{n}_{1x} (green line with dots), \bar{n}_{2x} (orange line with squares), \bar{n}_{1z} (light green dashed line with rhombuses), and \bar{n}_{2z} (yellow dashed line with triangles) versus the effective driving detuning $\Delta/\tilde{\omega}_{1x}$. Other parameters used are $\bar{n}_{1x,\text{th}} = \bar{n}_{2x,\text{th}} = \bar{n}_{1z,\text{th}} = \bar{n}_{2z,\text{th}} = 10^5$, $\tilde{\omega}_{2x}/\tilde{\omega}_{1x} \approx 0.75$, $\tilde{\omega}_{1z}/\tilde{\omega}_{1x} \approx 0.41$, $\tilde{\omega}_{2z}/\tilde{\omega}_{1x} \approx 0.31$, $G_x/\tilde{\omega}_{1x} \approx -0.02$, $G_z/\tilde{\omega}_{1x} \approx -0.03$, $G_{x_1}/\tilde{\omega}_{1x} \approx -0.1$, $G_{x_2}/\tilde{\omega}_{1x} \approx -0.09$, $\gamma_{1x}/\tilde{\omega}_{1x} = \gamma_{1z}/\tilde{\omega}_{1x} = \gamma_{2x}/\tilde{\omega}_{1x} = \gamma_{2z}/\tilde{\omega}_{1x} = 0.5 \times 10^{-8}$, and $\kappa/\tilde{\omega}_{1x} = 0.2$.

modes. Therefore, the cooling of the four mechanical modes will be significantly suppressed.

In order to break the dark-mode effect, we need to consider the case $P_{\text{tw}}^{(1)} \neq P_{\text{tw}}^{(2)}$, then we have $|g_z| > |g_x|$ and $\tilde{\omega}_z < \tilde{\omega}_x$ for our parameters. In the dark-mode-breaking case, we want to investigate the influence of the detuning on the cooling performance for the motions. In Fig. 8(a), we plot the final mean phonon numbers \bar{n}_{1x} , \bar{n}_{2x} , \bar{n}_{1z} , and \bar{n}_{2z} in the four mechanical modes versus the scaled detuning $\Delta/\tilde{\omega}_{1x}$. We find in Fig. 8(a) that the simultaneous ground-state cooling of the four mechanical modes can be realized. In particular, the cooling performance of the x -direction motions are better than those of the two modes z_1 and z_2 . Moreover, we can see from Fig. 8(a) that, for the two modes x_1 and x_2 , the optimal cooling appears respectively around $\Delta/\tilde{\omega}_{1x} \approx 1$ and $\Delta/\tilde{\omega}_{2x} \approx 0.75$, corresponding to the red-sideband resonances. In this case, the effective mode temperatures of the x -direction motions for the two nanoparticles are cooled to $T_x \sim 5 \times 10^{-3}$ mK (corresponding to $\tilde{\omega}_x \sim 2.4$ MHz), and the two z -mode mechanical oscillations are simultaneously cooled to $T_z \sim 7 \times 10^{-3}$ mK

(corresponding to $\tilde{\omega}_z \sim 0.9$ MHz). We also investigate the dependence of the final mean phonon numbers $\bar{n}_{1,x}$, $\bar{n}_{2,x}$, $\bar{n}_{1,z}$, and $\bar{n}_{2,z}$ on the scaled decay rate $\kappa/\tilde{\omega}_{1,x}$ for the cavity field, as shown by Fig. 8(b). Here, we can see that the simultaneous ground-state cooling of the four modes can be realized. In particular, the cooling performances of the two x -direction modes x_1 and x_2 are better than those of the two z -direction modes z_1 and z_2 . Meanwhile, we find that the main cooling region exists in the resolved-sideband regime.

V. DISCUSSIONS AND CONCLUSION

Finally, we present some discussions concerning the decoherence effect in this scheme. In reality, there exist some noise processes such as recoil heating, photon absorption, and laser phase noise. These noises will inevitably cause some system decoherence. In this work, we did not conduct quantitative analyses concerning the effect of these noises separately. We only consider that the cavity mode and each mechanical mode are coupled to a vacuum bath and a heat bath, respectively. We also consider a real dielectric constant (i.e., no absorption effects are taken into account). In addition, the heating noise originates from two contributions: one is the heating effect caused by the collision of the nanoparticles with surrounding gas molecules, the other one is the recoil heating caused by the collision of the nanoparticles with the photons escaped from the optical trap. According to Ref. [94], the ratio between the decoherence rate induced by the photon shot noise and thermal decoherence induced by the gas collision increases as the decrease of the vacuum pressure. In this work, we consider the case in which the decoherence induced by gas collisions dominates the heating processes, and hence the decoherence of the system can be described by the Langevin equations.

We should mention that the cooling performance depends on the initial thermal phonon numbers in these modes. In our simulations, we consider the initial phonon number $\bar{n}_{\text{th}} = 10^5$. We also conduct the simulations for a larger initial \bar{n}_{th} , for example $\bar{n}_{\text{th}} = 10^7$ corresponding to a room temperature for typical mechanical frequency. We find that the ground-state cooling for the x modes of the two nanoparticles can be realized at $\bar{n}_{\text{th}} = 10^7$. However, the ground-state cooling of the x and z modes of the two nanoparticles cannot be realized, but the final mean phonon numbers can be reduced to be smaller than 10 with the cooperativity $C_Q \approx 4g^2/(\kappa\gamma\bar{n}_{\text{th}}) \approx 4$.

We note that the normal-mode splitting caused by a strong optical binding [77] can limit the cooling efficiency. In particular, when the two coupled mechanical modes are working in the ultrastrong-coupling regime (namely the coupling strength is considerably comparable to the mechanical resonance frequency), the two mechanical oscillators should be treated as a whole system. Namely, the mechanical modes are no longer individually coupled to the thermal bath. Instead,

each of the two hybrid modes will be coupled to two environments, and hence the equations of motion governing the evolution of the two coupled mechanical modes should be re-derived in the dressed-mode representation. In other words, we need to consider this model in the normal-mode representation when the two coupled mechanical modes work in the ultrastrong-coupling regime. With the coupling between the two mechanical modes in the weak- and strong-coupling regimes, we can safely work in the bare-mode representation of the two mechanical modes. In our simulations, we consider this coupling strength $G_x \approx -0.045\Omega_1$ in the strong-coupling regime. Therefore, our treatment and calculations are valid for our used parameters.

In conclusion, we have developed a theoretical model for describing the simultaneous ground-state cooling of the motions of two levitated nanoparticles trapped in a cavity via coherent scattering. We have found that, different from the single-levitated particle case, the scattered light will induce the mechanical effect between the particles, which shifts the equilibrium position of the particles and causes the coupling between two particles. We have derived the Hamiltonian of the system and analyze the interactions in various cases. When the two nanoparticles are located at the nodes of the cavity, the system is reduced to a three-mode loop-coupled model, in which the cavity mode is coupled to the x -direction motional modes of the two particles, and the two x modes are coupled with each other via the position-position coupling. In this case, we have found that the dark-mode effect appears when two tweezers have the same power, and then the effective cooling of the two mechanical oscillations is suppressed. In particular, the simultaneous ground-state cooling of the x -direction motion of the two particles can be realized by breaking the dark-mode effect. In addition, when the particles are not placed at the nodes, the system is reduced to a five-mode model, in which both the x - and z -direction motions are coupled to the cavity mode, and there exist both the x - x coupling and z - z coupling between the two mechanical modes. In this case, we have also found that the dark-mode effect exists in the identical-power case, and that both the x - and z -direction motions can be significantly cooled by breaking the dark-mode effect. This work paves the way to quantum manipulation of multiple levitated nanoparticles.

ACKNOWLEDGMENTS

J.-Q.L. was supported in part by National Natural Science Foundation of China (Grants No. 12175061, No. 12247105, and No. 11935006), the Science and Technology Innovation Program of Hunan Province (Grant No. 2021RC4029), and Hunan Provincial Major Science and Technology Program (Grant No. 2023ZJ1010).

Appendix: Expansions of these interaction Hamiltonians described by Eqs. (21)

In this Appendix, we present the derivation of these interaction Hamiltonians given by Eqs. (21). We start by substituting Eqs. (9) and (11) into Eq. (21a), and obtain

$$\begin{aligned}
\hat{H}_{\text{tw-Gtw}}^{(1)} &= -\alpha \mathcal{E}_{\text{tw1}}(\hat{\mathbf{R}}_1, t) \cdot \text{Re}[e^{ik_{\text{tw}}\hat{R}_0} \eta_{f_{\text{tw}}}(D/\hat{R}_0) \overleftrightarrow{\mathbf{M}}_f(\hat{\mathbf{R}}_0) \cdot \mathbf{E}_{\text{tw2}}(\hat{\mathbf{R}}_2, t)] \\
&= -\alpha \left[\frac{1}{2} E_{10}(\hat{\mathbf{R}}_1) e^{-ik_{\text{tw}}\hat{Z}_1} e^{-i\omega_{\text{tw}}t} + \frac{1}{2} E_{10}(\hat{\mathbf{R}}_1) e^{ik_{\text{tw}}\hat{Z}_1} e^{i\omega_{\text{tw}}t} \right] \mathbf{e}_{\text{tw}}^{(1)} \cdot \text{Re}[e^{ik_{\text{tw}}\hat{R}_0} \eta_{f_{\text{tw}}}(D/\hat{R}_0) \overleftrightarrow{\mathbf{M}}_f(\hat{\mathbf{R}}_0) \cdot E_{20}(\hat{\mathbf{R}}_2) e^{-ik_{\text{tw}}\hat{Z}_2} e^{-i\omega_{\text{tw}}t} \mathbf{e}_{\text{tw}}^{(2)}] \\
&\approx -\frac{1}{2} \alpha \eta_{f_{\text{tw}}}(D/\hat{R}_0) \left[\frac{1}{2} E_{10}(\hat{\mathbf{R}}_1) E_{20}(\hat{\mathbf{R}}_2) e^{-ik_{\text{tw}}\hat{R}_0} e^{-ik_{\text{tw}}(\hat{Z}_1 - \hat{Z}_2)} + \frac{1}{2} E_{10}(\hat{\mathbf{R}}_1) E_{20}(\hat{\mathbf{R}}_2) e^{ik_{\text{tw}}\hat{R}_0} e^{ik_{\text{tw}}(\hat{Z}_1 - \hat{Z}_2)} \right] \mathbf{e}_{\text{tw}}^{(1)} \cdot \overleftrightarrow{\mathbf{M}}_f(\hat{\mathbf{R}}_0) \cdot \mathbf{e}_{\text{tw}}^{(2)} \\
&= -\frac{1}{2} \alpha \eta_{f_{\text{tw}}}(D/\hat{R}_0) E_{10}(\hat{\mathbf{R}}_1) E_{20}(\hat{\mathbf{R}}_2) \cos(-k_{\text{tw}}\hat{Z}_0 - k_{\text{tw}}\hat{R}_0) \mathbf{e}_{\text{tw}}^{(1)} \cdot \overleftrightarrow{\mathbf{M}}_f(\hat{\mathbf{R}}_0) \cdot \mathbf{e}_{\text{tw}}^{(2)}, \tag{A.1}
\end{aligned}$$

where we neglect the fast-oscillating terms by performing the rotating-wave approximation. Similarly, we can obtain the Hamiltonian

$$\begin{aligned}
\hat{H}_{\text{tw-Gtw}}^{(2)} &= -\alpha \mathcal{E}_{\text{tw2}}(\hat{\mathbf{R}}_2, t) \cdot \text{Re}[e^{ik_{\text{tw}}\hat{R}_0} \eta_{f_{\text{tw}}}(D/\hat{R}_0) \overleftrightarrow{\mathbf{M}}_f(\hat{\mathbf{R}}_0) \cdot \mathbf{E}_{\text{tw1}}(\hat{\mathbf{R}}_1, t)] \\
&\approx -\frac{1}{2} \alpha \eta_{f_{\text{tw}}}(D/\hat{R}_0) E_{20}(\hat{\mathbf{R}}_2) E_{10}(\hat{\mathbf{R}}_1) \cos(k_{\text{tw}}\hat{Z}_0 - k_{\text{tw}}\hat{R}_0) \mathbf{e}_{\text{tw}}^{(2)} \cdot \overleftrightarrow{\mathbf{M}}_f(\hat{\mathbf{R}}_0) \cdot \mathbf{e}_{\text{tw}}^{(1)}. \tag{A.2}
\end{aligned}$$

Based on Eqs. (A.1) and (A.2), the Hamiltonian $\hat{H}_{\text{tw-Gtw}}$ given in Eq. (24) can be derived. Since the j th particle is trapped near the focus of the j th tweezer, we can approximate the electric field by its expansion near the foci $r_{10} = (x_{10}, 0, 0)$ and $r_{20} = (x_{20}, 0, 0)$ of the two tweezers. The approximate Hamiltonian expanded up to the second order of the center-of-mass displacements is given by Eq. (25).

In the rotating frame with respect to $U = \exp(-i\omega_{\text{tw}}\hat{a}^\dagger \hat{a} t)$, the electric field operator of the cavity field can be expressed as $\hat{\mathbf{E}}_{\text{cav}}(\hat{\mathbf{R}}_j) = \epsilon_{\text{cav}} \cos(k\hat{X}_j) (\hat{a}^\dagger e^{i\omega_{\text{tw}}t} + \hat{a} e^{-i\omega_{\text{tw}}t}) \mathbf{e}_{\text{cav}}$. By substituting $\hat{\mathbf{E}}_{\text{cav}}(\hat{\mathbf{R}}_j)$ into Eq. (21b) for $j = 1$, we obtain

$$\begin{aligned}
\hat{H}_{\text{cav-Gcav}}^{(1)} &= -\alpha \hat{\mathbf{E}}_{\text{cav}}(\hat{\mathbf{R}}_1) \cdot \text{Re}[e^{ik\hat{R}_0} \eta_f(D/\hat{R}_0) \overleftrightarrow{\mathbf{M}}_f(\hat{\mathbf{R}}_0) \cdot \hat{\mathbf{E}}_{\text{cav}}(\hat{\mathbf{R}}_2)] \\
&= -\alpha \epsilon_{\text{cav}} \cos(k\hat{X}_1) (\hat{a}^\dagger e^{i\omega_{\text{tw}}t} + \hat{a} e^{-i\omega_{\text{tw}}t}) \mathbf{e}_{\text{cav}} \cdot \text{Re}[e^{ik\hat{R}_0} \eta_f(D/\hat{R}_0) \overleftrightarrow{\mathbf{M}}_f(\hat{\mathbf{R}}_0) \cdot \epsilon_{\text{cav}} \cos(k\hat{X}_2) (\hat{a}^\dagger e^{i\omega_{\text{tw}}t} + \hat{a} e^{-i\omega_{\text{tw}}t}) \mathbf{e}_{\text{cav}}] \\
&\approx -2\alpha \epsilon_{\text{cav}}^2 \eta_f(D/\hat{R}_0) \cos(k\hat{X}_1) \cos(k\hat{X}_2) \cos(k\hat{R}_0) (\hat{a}^\dagger \hat{a} + 1/2) \mathbf{e}_{\text{cav}} \cdot \overleftrightarrow{\mathbf{M}}_f(\hat{\mathbf{R}}_0) \cdot \mathbf{e}_{\text{cav}}. \tag{A.3}
\end{aligned}$$

Similarly, we can obtain

$$\begin{aligned}
\hat{H}_{\text{cav-Gcav}}^{(2)} &= -\alpha \hat{\mathbf{E}}_{\text{cav}}(\hat{\mathbf{R}}_2) \cdot \text{Re}[e^{ik\hat{R}_0} \eta_f(D/\hat{R}_0) \overleftrightarrow{\mathbf{M}}_f(\hat{\mathbf{R}}_0) \cdot \hat{\mathbf{E}}_{\text{cav}}(\hat{\mathbf{R}}_1)] \\
&\approx -2\alpha \epsilon_{\text{cav}}^2 \eta_f(D/\hat{R}_0) \cos(k\hat{X}_2) \cos(k\hat{X}_1) \cos(k\hat{R}_0) (\hat{a}^\dagger \hat{a} + 1/2) \mathbf{e}_{\text{cav}} \cdot \overleftrightarrow{\mathbf{M}}_f(\hat{\mathbf{R}}_0) \cdot \mathbf{e}_{\text{cav}}. \tag{A.4}
\end{aligned}$$

In terms of Eqs. (A.3) and (A.4), we obtain the expression of $\hat{H}_{\text{cav-Gcav}}$, which has been presented in Eq. (29). By expanding the Hamiltonian with respect to the center-of-mass displacements, we reach the approximate Hamiltonian

$$\begin{aligned}
\hat{H}_{\text{cav-Gcav}} &\approx -4\alpha \epsilon_{\text{cav}}^2 \eta_f \cos(kx_{10}) \cos(kx_{20}) \cos(kD) \hat{a}^\dagger \hat{a} \\
&\quad + 4\alpha \epsilon_{\text{cav}}^2 \eta_f \{ [k \sin(kD) + \cos(kD)]/D \} \cos(kx_{10}) \cos(kx_{20}) + k \sin(kx_{10}) \cos(kx_{20}) \cos(kD) \} \hat{x}_1 (\hat{a}^\dagger \hat{a} + 1/2) \\
&\quad - 4\alpha \epsilon_{\text{cav}}^2 \eta_f \{ [k \sin(kD) + \cos(kD)]/D \} \cos(kx_{10}) \cos(kx_{20}) - k \cos(kx_{10}) \sin(kx_{20}) \cos(kD) \} \hat{x}_2 (\hat{a}^\dagger \hat{a} + 1/2) \\
&\quad + \mathcal{O}(\hat{Q}_j^2), \tag{A.5}
\end{aligned}$$

where $\hat{Q}_j = \hat{x}_j, \hat{y}_j, \hat{z}_j$. By keeping the terms up to the first order of the center-of-mass displacements and taking $x_{10} = D/2$ and $x_{20} = -D/2$, Eq. (A.5) is reduced to Eq. (30).

Substituting the tweezer fields and the cavity field into Eq. (21c), we can obtain the Hamiltonian

$$\begin{aligned}
\hat{H}_{\text{tw-Gcav}}^{(1)} &= -\alpha \mathcal{E}_{\text{tw1}}(\hat{\mathbf{R}}_1, t) \cdot \text{Re}[e^{ik\hat{R}_0} \eta_f(D/\hat{R}_0) \overleftrightarrow{\mathbf{M}}_f(\hat{\mathbf{R}}_0) \cdot \hat{\mathbf{E}}_{\text{cav}}(\hat{\mathbf{R}}_2)] \\
&= -\alpha \text{Re}[E_{10}(\hat{\mathbf{R}}_1) e^{-ik_{\text{tw}}\hat{Z}_1} e^{-i\omega_{\text{tw}}t}] \mathbf{e}_{\text{tw}}^{(1)} \cdot \text{Re}[e^{ik\hat{R}_0} \eta_f(D/\hat{R}_0) \overleftrightarrow{\mathbf{M}}_f(\hat{\mathbf{R}}_0) \cdot \epsilon_{\text{cav}} \cos(k\hat{X}_2) (\hat{a}^\dagger e^{i\omega_{\text{tw}}t} + \hat{a} e^{-i\omega_{\text{tw}}t}) \mathbf{e}_{\text{cav}}] \\
&\approx -\frac{1}{2} \alpha \eta_f \epsilon_{\text{cav}} (D/\hat{R}_0) \cos(k\hat{R}_0) E_{10}(\hat{\mathbf{R}}_1) \cos(k\hat{X}_2) (\hat{a}^\dagger e^{-ik_{\text{tw}}\hat{Z}_1} + \hat{a} e^{ik_{\text{tw}}\hat{Z}_1}) \mathbf{e}_{\text{tw}}^{(1)} \cdot \overleftrightarrow{\mathbf{M}}_f(\hat{\mathbf{R}}_0) \cdot \mathbf{e}_{\text{cav}}, \tag{A.6}
\end{aligned}$$

and

$$\begin{aligned}\hat{H}_{\text{tw-Gcav}}^{(2)} &= -\alpha \mathcal{E}_{\text{tw2}}(\hat{\mathbf{R}}_2, t) \cdot \text{Re}[e^{ik\hat{R}_0} \eta_f(D/\hat{R}_0) \overleftrightarrow{\mathbf{M}}_f(\hat{\mathbf{R}}_0) \cdot \hat{\mathbf{E}}_{\text{cav}}(\hat{\mathbf{R}}_1)] \\ &\approx -\frac{1}{2} \alpha \eta_f \epsilon_{\text{cav}}(D/\hat{R}_0) \cos(k\hat{R}_0) E_{20}(\hat{\mathbf{R}}_2) \cos(k\hat{X}_1) (\hat{a}^\dagger e^{-ik_{\text{tw}}\hat{Z}_2} + \hat{a} e^{ik_{\text{tw}}\hat{Z}_2}) \mathbf{e}_{\text{tw}}^{(2)} \cdot \overleftrightarrow{\mathbf{M}}_f(\hat{\mathbf{R}}_0) \cdot \mathbf{e}_{\text{cav}}.\end{aligned}\quad (\text{A.7})$$

Combining Eqs. (A.6) and (A.7), we can obtain the form of $\hat{H}_{\text{tw-Gcav}}$, as shown in Eq. (32). Then we get the approximate Hamiltonian by expanding the fields near the foci of the tweezers,

$$\begin{aligned}\hat{H}_{\text{tw-Gcav}} &\approx -\frac{1}{2} \alpha \eta_f \epsilon_{\text{cav}} \cos(kD) \varsigma (\hat{a}^\dagger + \hat{a}) \\ &\quad + \frac{1}{2} \alpha \eta_f \epsilon_{\text{cav}} \left\{ [k \sin(kD) + \cos(kD)/D] \varsigma + \epsilon_{\text{tw}}^{(2)} k \cos(kD) \sin(kx_{10}) \right\} (\hat{a}^\dagger + \hat{a}) \hat{x}_1 \\ &\quad - \frac{1}{2} \alpha \eta_f \epsilon_{\text{cav}} \left\{ [k \sin(kD) + \cos(kD)/D] \varsigma - \epsilon_{\text{tw}}^{(1)} k \cos(kD) \sin(kx_{20}) \right\} (\hat{a}^\dagger + \hat{a}) \hat{x}_2 \\ &\quad - \frac{i}{2} \alpha \eta_f \epsilon_{\text{cav}} \epsilon_{\text{tw}}^{(1)} \cos(kD) k_{\text{tw}} \cos(kx_{20}) (\hat{a} - \hat{a}^\dagger) \hat{z}_1 - \frac{i}{2} \alpha \eta_f \epsilon_{\text{cav}} \epsilon_{\text{tw}}^{(2)} \cos(kD) k_{\text{tw}} \cos(kx_{10}) (\hat{a} - \hat{a}^\dagger) \hat{z}_2 \\ &\quad + \mathcal{O}(\hat{Q}_j^2),\end{aligned}\quad (\text{A.8})$$

with $\varsigma = \epsilon_{\text{tw}}^{(1)} \cos(kx_{20}) + \epsilon_{\text{tw}}^{(2)} \cos(kx_{10})$. We keep the terms up to the first order of the center-of-mass displacements and obtain Eq. (33).

Similarly, using the expressions of the two electric fields, we can further express Eq. (21d) as

$$\begin{aligned}\hat{H}_{\text{cav-Gtw}}^{(1)} &= -\alpha \hat{\mathbf{E}}_{\text{cav}}(\hat{\mathbf{R}}_1) \cdot \text{Re}[e^{ik_{\text{tw}}\hat{R}_0} \eta_{f_{\text{tw}}}(D/\hat{R}_0) \overleftrightarrow{\mathbf{M}}_{f_{\text{tw}}}(\hat{\mathbf{R}}_0) \cdot \mathbf{E}_{\text{tw2}}(\hat{\mathbf{R}}_2, t)] \\ &= -\alpha \epsilon_{\text{cav}} \cos(k\hat{X}_1) (\hat{a}^\dagger e^{i\omega_{\text{tw}}t} + \hat{a} e^{-i\omega_{\text{tw}}t}) \mathbf{e}_{\text{cav}} \cdot \text{Re}[e^{ik_{\text{tw}}\hat{R}_0} \eta_{f_{\text{tw}}}(D/\hat{R}_0) \overleftrightarrow{\mathbf{M}}_{f_{\text{tw}}}(\hat{\mathbf{R}}_0) \cdot E_{20}(\hat{\mathbf{R}}_2) e^{-ik_{\text{tw}}\hat{Z}_2} e^{-i\omega_{\text{tw}}t} \mathbf{e}_{\text{tw}}^{(2)}] \\ &\approx -\frac{1}{2} \alpha \eta_{f_{\text{tw}}} \epsilon_{\text{cav}}(D/\hat{R}_0) \cos(k\hat{X}_1) E_{20}(\hat{\mathbf{R}}_2) [\hat{a}^\dagger e^{ik_{\text{tw}}(\hat{R}_0 - \hat{Z}_2)} - \hat{a} e^{-ik_{\text{tw}}(\hat{R}_0 - \hat{Z}_2)}] \mathbf{e}_{\text{cav}} \cdot \overleftrightarrow{\mathbf{M}}_{f_{\text{tw}}}(\hat{\mathbf{R}}_0) \cdot \mathbf{e}_{\text{tw}}^{(2)},\end{aligned}\quad (\text{A.9})$$

and

$$\begin{aligned}\hat{H}_{\text{cav-Gtw}}^{(2)} &= -\alpha \hat{\mathbf{E}}_{\text{cav}}(\hat{\mathbf{R}}_2) \cdot \text{Re}[e^{ik_{\text{tw}}\hat{R}_0} \eta_{f_{\text{tw}}}(D/\hat{R}_0) \overleftrightarrow{\mathbf{M}}_{f_{\text{tw}}}(\hat{\mathbf{R}}_0) \cdot \mathbf{E}_{\text{tw1}}(\hat{\mathbf{R}}_1, t)] \\ &\approx -\frac{1}{2} \alpha \eta_{f_{\text{tw}}} \epsilon_{\text{cav}}(D/\hat{R}_0) \cos(k\hat{X}_2) E_{10}(\hat{\mathbf{R}}_1) [\hat{a}^\dagger e^{ik_{\text{tw}}(\hat{R}_0 - \hat{Z}_1)} + \hat{a} e^{-ik_{\text{tw}}(\hat{R}_0 - \hat{Z}_1)}] \mathbf{e}_{\text{cav}} \cdot \overleftrightarrow{\mathbf{M}}_{f_{\text{tw}}}(\hat{\mathbf{R}}_0) \cdot \mathbf{e}_{\text{tw}}^{(1)}.\end{aligned}\quad (\text{A.10})$$

From Eqs. (A.9) and (A.10), we derive the expression of $\hat{H}_{\text{cav-Gtw}}$ as presented in Eq. (35). By expanding the electric fields close to the foci of the tweezers, the Hamiltonian becomes

$$\begin{aligned}\hat{H}_{\text{cav-Gtw}} &\approx -\frac{1}{2} \alpha \eta_{f_{\text{tw}}} \epsilon_{\text{cav}} \varsigma (\hat{a} e^{-ik_{\text{tw}}D} + \hat{a}^\dagger e^{ik_{\text{tw}}D}) \\ &\quad + \frac{1}{2} \alpha \eta_{f_{\text{tw}}} \epsilon_{\text{cav}} \left\{ [(D^{-1} + ik_{\text{tw}}) \varsigma + \epsilon_{\text{tw}}^{(2)} k \sin(kx_{10})] \hat{a} e^{-ik_{\text{tw}}D} + [(D^{-1} - ik_{\text{tw}}) \varsigma + \epsilon_{\text{tw}}^{(2)} k \sin(kx_{10})] \hat{a}^\dagger e^{ik_{\text{tw}}D} \right\} \hat{x}_1 \\ &\quad + \frac{1}{2} \alpha \eta_{f_{\text{tw}}} \epsilon_{\text{cav}} \left\{ [(D^{-1} + ik_{\text{tw}}) \varsigma + \epsilon_{\text{tw}}^{(1)} k \sin(kx_{20})] \hat{a} e^{-ik_{\text{tw}}D} + [(D^{-1} - ik_{\text{tw}}) \varsigma + \epsilon_{\text{tw}}^{(1)} k \sin(kx_{20})] \hat{a}^\dagger e^{ik_{\text{tw}}D} \right\} \hat{x}_2 \\ &\quad - \frac{i}{2} \alpha \eta_{f_{\text{tw}}} \epsilon_{\text{cav}} \epsilon_{\text{tw}}^{(1)} k_{\text{tw}} \cos(kx_{20}) (\hat{a} e^{-ik_{\text{tw}}D} - \hat{a}^\dagger e^{ik_{\text{tw}}D}) \hat{z}_1 - \frac{i}{2} \alpha \eta_{f_{\text{tw}}} \epsilon_{\text{cav}} \epsilon_{\text{tw}}^{(2)} k_{\text{tw}} \cos(kx_{10}) (\hat{a} e^{-ik_{\text{tw}}D} - \hat{a}^\dagger e^{ik_{\text{tw}}D}) \hat{z}_2 \\ &\quad + \mathcal{O}(\hat{Q}_j^2).\end{aligned}\quad (\text{A.11})$$

Discarding the last term in Eq. (A.11), we reach the Hamiltonian given by Eq. (36).

-
- [1] M. Aspelmeyer, T. J. Kippenberg, and F. Marquardt, Cavity optomechanics, *Rev. Mod. Phys.* **86**, 1391 (2014).
 [2] M. Metcalfe, Applications of Cavity Optomechanics, *Appl.*

- Phys. Rev.* **1**, 031105 (2014).
 [3] J. Millen, T. S. Monteiro, R. Pettit, and A. N. Vamivakas, Optomechanics with levitated particles, *Rep. Prog. Phys.* **83**,

- 026401 (2020).
- [4] C. Gonzalez-Ballester, M. Aspelmeyer, L. Novotny, R. Quidant, and O. Romero-Isart, Levitodynamics: Levitation and control of microscopic objects in vacuum, *Science* **374**, eabg3027 (2021).
- [5] G. Winstone, M. Bhattacharya, A. A. Geraci, T. Li, P. J. Pauzauskie, and N. Vamivakas, Levitated optomechanics: A tutorial and perspective, arXiv: 2307.11858.
- [6] A. Ashkin, Acceleration and Trapping of Particles by Radiation Pressure, *Phys. Rev. Lett.* **24**, 156 (1970).
- [7] A. Ashkin and J. Dziedzic, Optical Levitation by Radiation Pressure, *Appl. Phys. Lett.* **19**, 283 (1971).
- [8] A. Ashkin, J. M. Dziedzic, J. E. Bjorkholm, and S. Chu, Observation of a single-beam gradient force optical trap for dielectric particles, *Opt. Lett.* **11**, 288 (1986).
- [9] W. D. Phillips, Nobel lecture: Laser cooling and trapping of neutral atoms, *Rev. Mod. Phys.* **70**, 721 (1998).
- [10] T. Delord, P. Huillery, L. Nicolas, and G. Hétet, Spin-cooling of the motion of a trapped diamond, *Nature (London)* **580**, 56 (2020).
- [11] T. Li, S. Kheifets, D. Medellin, and M. G. Raizen, Measurement of the instantaneous velocity of a Brownian particle, *Science* **328**, 1673 (2010).
- [12] U. Delić, M. Reisenbauer, K. Dare, D. Grass, V. Vuletić, N. Kiesel, and M. Aspelmeyer, Cooling of a levitated nano-particle to the motional quantum ground state, *Science* **367**, 892 (2020).
- [13] L. Magrini, P. Rosenzweig, C. Bach, A. Deutschmann-Olek, S. G. Hofer, S. Hong, N. Kiesel, A. Kugi, and M. Aspelmeyer, Real-time optimal quantum control of mechanical motion at room temperature, *Nature (London)* **595**, 373 (2021).
- [14] F. Tebbenjohanns, M. L. Mattana, M. Rossi, M. Frimmer, and L. Novotny, Quantum control of a nanoparticle optically levitated in cryogenic free space, *Nature (London)* **595**, 378 (2021).
- [15] F. Monteiro, S. Ghosh, A. G. Fine, and D. C. Moore, Optical levitation of 10-ng spheres with nano-g acceleration sensitivity, *Phys. Rev. A* **96**, 063841 (2017).
- [16] A. D. Rider, C. P. Blakemore, G. Gratta, and D. C. Moore, Single-beam dielectric-microsphere trapping with optical heterodyne detection, *Phys. Rev. A* **97**, 013842 (2018).
- [17] Y. Zheng, L.-M. Zhou, Y. Dong, C.-W. Qiu, X.-D. Chen, G.-C. Guo, and F.-W. Sun, Robust Optical-Levitation-Based Metrology of Nanoparticle's Position and Mass, *Phys. Rev. Lett.* **124**, 223603 (2020).
- [18] R. Reimann, M. Doderer, E. Hebestreit, R. Diehl, M. Frimmer, D. Windey, F. Tebbenjohanns, and L. Novotny, GHz Rotation of an Optically Trapped Nanoparticle in Vacuum, *Phys. Rev. Lett.* **121**, 033602 (2018).
- [19] J. Ahn, Z. Xu, J. Bang, Y.-H. Deng, T. M. Hoang, Q. Han, R.-M. Ma, and T. Li, Optically Levitated Nanodumbbell Torsion Balance and GHz Nanomechanical Rotor, *Phys. Rev. Lett.* **121**, 033603 (2018).
- [20] D. E. Chang, C. A. Regal, S. B. Papp, D. J. Wilson, J. Ye, O. Painter, H. J. Kimble, and P. Zoller, Cavity opto-mechanics using an optically levitated nanosphere, *Proc. Natl. Acad. Sci. U.S.A.* **107**, 1005 (2010).
- [21] O. Romero-Isart, M. L. Juan, R. Quidant, and J. I. Cirac, Toward quantum superposition of living organisms, *New J. Phys.* **12**, 033015 (2010).
- [22] T. Li, S. Kheifets, and M. G. Raizen, Millikelvin cooling of an optically trapped microsphere in vacuum, *Nat. Phys.* **7**, 527 (2011).
- [23] A. A. Geraci, S. B. Papp, and J. Kitching, Short-Range Force Detection Using Optically Cooled Levitated Microspheres, *Phys. Rev. Lett.* **105**, 101101 (2010).
- [24] J. Gieseler, B. Deutsch, R. Quidant, and L. Novotny, Subkelvin Parametric Feedback Cooling of a Laser-Trapped Nanoparticle, *Phys. Rev. Lett.* **109**, 103603 (2012).
- [25] N. Kiesel, F. Blaser, U. Delić, D. Grass, R. Kaltenbaek, and M. Aspelmeyer, Cavity cooling of an optically levitated submicron particle, *Proc. Natl. Acad. Sci. U.S.A.* **110**, 14180 (2013).
- [26] J. Millen, T. Deesuwan, P. Barker, and J. Anders, Nanoscale temperature measurements using non-equilibrium Brownian dynamics of a levitated nanosphere, *Nat. Nanotechnol.* **9**, 425 (2014).
- [27] D. C. Moore and A. A. Geraci, Searching for new physics using optically levitated sensors, *Quantum Sci. Technol.* **6**, 014008 (2021).
- [28] T. F. Kuang, R. Huang, W. Xiong, Y. L. Zuo, X. Han, F. Nori, C.-W. Qiu, H. Luo, H. Jing, and G. Z. Xiao, Nonlinear multi-frequency phonon lasers with active levitated optomechanics, *Nat. Phys.* **19**, 414 (2023).
- [29] U. Delić, D. Grass, M. Reisenbauer, T. Damm, M. Weitz, N. Kiesel, and M. Aspelmeyer, Levitated cavity optomechanics in high vacuum, *Quantum Sci. Technol.* **5**, 025006 (2020).
- [30] I. Wilson-Rae, N. Nooshi, W. Zwerger, and T. J. Kippenberg, Theory of Ground State Cooling of a Mechanical Oscillator Using Dynamical Backaction, *Phys. Rev. Lett.* **99**, 093901 (2007).
- [31] F. Marquardt, J. P. Chen, A. A. Clerk, and S. M. Girvin, Quantum Theory of Cavity-Assisted Sideband Cooling of Mechanical Motion, *Phys. Rev. Lett.* **99**, 093902 (2007).
- [32] J. Chan, T. P. M. Alegre, A. H. Safavi-Naeini, J. T. Hill, A. Krause, S. Gröblacher, M. Aspelmeyer, and O. Painter, Laser cooling of a nanomechanical oscillator into its quantum ground state, *Nature (London)* **478**, 89 (2011).
- [33] C. Sommer and C. Genes, Partial Optomechanical Refrigeration via Multimode Cold-Damping Feedback, *Phys. Rev. Lett.* **123**, 203605 (2019).
- [34] Y.-H. Liu, X.-L. Yin, J.-F. Huang, and J.-Q. Liao, Accelerated ground-state cooling of an optomechanical resonator via shortcuts to adiabaticity, *Phys. Rev. A* **105**, 023504 (2022).
- [35] R. Diehl, E. Hebestreit, R. Reimann, F. Tebbenjohanns, M. Frimmer, and L. Novotny, Optical levitation and feedback cooling of a nanoparticle at subwavelength distances from a membrane, *Phys. Rev. A* **98**, 013851 (2018).
- [36] G. P. Conangla, F. Ricci, M. T. Cuairan, A. W. Schell, N. Meyer, and R. Quidant, Optimal Feedback Cooling of a Charged Levitated Nanoparticle with Adaptive Control, *Phys. Rev. Lett.* **122**, 223602 (2019).
- [37] F. Tebbenjohanns, M. Frimmer, A. Militaru, V. Jain, and L. Novotny, Cold Damping of an Optically Levitated Nanoparticle to Microkelvin Temperatures, *Phys. Rev. Lett.* **122**, 223601 (2019).
- [38] P. F. Barker and M. N. Schneider, Cavity cooling of an optically trapped nanoparticle, *Phys. Rev. A* **81**, 023826 (2010).
- [39] O. Romero-Isart, A. C. Pflanzer, M. L. Juan, R. Quidant, N. Kiesel, M. Aspelmeyer, and J. I. Cirac, Optically levitating dielectrics in the quantum regime: Theory and protocols, *Phys. Rev. A* **83**, 013803 (2011).
- [40] P. Asenbaum, S. Kuhn, S. Nimmrichter, U. Sezer, and M. Arndt, Cavity cooling of free silicon nanoparticles in high vacuum, *Nat. Commun.* **4**, 2743 (2013).
- [41] J. Millen, P. Z. G. Fonseca, T. Mavrogordatos, T. S. Monteiro, and P. F. Barker, Cavity Cooling a Single Charged Levitated Nanosphere, *Phys. Rev. Lett.* **114**, 123602 (2015).
- [42] P. Z. G. Fonseca, E. B. Aranas, J. Millen, T. S. Monteiro, and P. F. Barker, Nonlinear Dynamics and Strong Cavity Cooling of Levitated Nanoparticles, *Phys. Rev. Lett.* **117**, 173602 (2016).
- [43] A. Ranfagni, K. Børkje, F. Marino, and F. Marin, Two-

- dimensional quantum motion of a levitated nanosphere, *Phys. Rev. Research* **4**, 033051 (2022).
- [44] N. Meyer, A. de los Ríos Sommer, P. Mestres, J. Gieseler, V. Jain, L. Novotny, and R. Quidant, Resolved-Sideband Cooling of a Levitated Nanoparticle in the Presence of Laser Phase Noise, *Phys. Rev. Lett.* **123**, 153601 (2019).
- [45] P. Rabl, C. Genes, K. Hammerer, and M. Aspelmeyer, Phase-noise induced limitations on cooling and coherent evolution in optomechanical systems, *Phys. Rev. A* **80**, 063819 (2009).
- [46] A. M. Jayich, J. C. Sankey, K. Børkje, D. Lee, C. Yang, M. Underwood, L. Childress, A. Petrenko, S. M. Girvin, and J. G. E. Harris, Cryogenic optomechanics with a Si_3N_4 membrane and classical laser noise, *New J. Phys.* **14**, 115018 (2012).
- [47] A. H. Safavi-Naeini, J. Chan, J. T. Hill, S. Gröblacher, H. Miao, Y. Chen, M. Aspelmeyer, and O. Painter, Laser noise in cavity-optomechanical cooling and thermometry, *New J. Phys.* **15**, 035007 (2013).
- [48] U. Delić, M. Reisenbauer, D. Grass, N. Kiesel, V. Vuletić, and M. Aspelmeyer, Cavity Cooling of a Levitated Nanosphere by Coherent Scattering, *Phys. Rev. Lett.* **122**, 123602 (2019).
- [49] D. Windey, C. Gonzalez-Ballester, P. Maurer, L. Novotny, O. Romero-Isart, and R. Reimann, Cavity-Based 3D Cooling of a Levitated Nanoparticle via Coherent Scattering, *Phys. Rev. Lett.* **122**, 123601 (2019).
- [50] C. Gonzalez-Ballester, P. Maurer, D. Windey, L. Novotny, R. Reimann, and O. Romero-Isart, Theory for cavity cooling of levitated nanoparticles via coherent scattering: Master equation approach, *Phys. Rev. A* **100**, 013805 (2019).
- [51] J. Piotrowski, D. Windey, J. Vijayan, C. Gonzalez-Ballester, A. de los Ríos Sommer, N. Meyer, R. Quidant, O. Romero-Isart, R. Reimann, and L. Novotny, Simultaneous ground-state cooling of two mechanical modes of a levitated nanoparticle, *Nat. Phys.* **19**, 1009 (2023).
- [52] V. Vuletić and S. Chu, Laser Cooling of Atoms, Ions, or Molecules by Coherent Scattering, *Phys. Rev. Lett.* **84**, 3787 (2000).
- [53] A. de los Ríos Sommer, N. Meyer, and R. Quidant, Strong optomechanical coupling at room temperature by coherent scattering, *Nat. Commun.* **12**, 276 (2021).
- [54] K. Dare, J. J. Hansen, I. Coroli, A. Johnson, M. Aspelmeyer, and U. Delić, Linear Ultrastrong Optomechanical Interaction, arXiv:2305.16226.
- [55] C. Marletto and V. Vedral, Gravitationally Induced Entanglement between Two Massive Particles is Sufficient Evidence of Quantum Effects in Gravity, *Phys. Rev. Lett.* **119**, 240402 (2017).
- [56] Y. Arita, E. M. Wright, and K. Dholakia, Optical Binding of two cooled micro-gyroscopes levitated in vacuum, *Optica* **5**, 910 (2018).
- [57] H. Rudolph, K. Hornberger, and B. A. Stickler, Entangling levitated nanoparticles by coherent scattering, *Phys. Rev. A* **101**, 011804(R) (2020).
- [58] A. K. Chauhan, O. Černotík, and R. Filip, Stationary Gaussian entanglement between levitated nanoparticles, *New J. Phys.* **22**, 123021 (2020).
- [59] V. Svak, J. Flajšmanová, L. Chvátal, M. Šiler, A. Jonáš, J. Ježek, S. H. Simpson, P. Zemánek, and O. Brzobohatý, Stochastic dynamics of optically bound matter levitated in vacuum, *Optica* **8**, 220 (2021).
- [60] Y. Arita, G. D. Bruce, E. M. Wright, S. H. Simpson, P. Zemánek, and K. Dholakia, All-optical sub-Kelvin sympathetic cooling of a levitated microsphere in vacuum, *Optica* **9**, 1000 (2022).
- [61] H. Rudolph, U. Delić, M. Aspelmeyer, K. Hornberger, and B. A. Stickler, Force-Gradient Sensing and Entanglement via Feedback Cooling of Interacting Nanoparticles, *Phys. Rev. Lett.* **129**, 193602 (2022).
- [62] T. W. Penny, A. Pontin, and P. F. Barker, Sympathetic cooling and squeezing of two colevitated nanoparticles, *Phys. Rev. Research* **5**, 013070 (2023).
- [63] H. Rudolph, U. Delić, K. Hornberger, and B. A. Stickler, Quantum theory of non-hermitian optical binding between nanoparticles, arXiv:2306.11893.
- [64] J. Vijayan, J. Piotrowski, C. Gonzalez-Ballester, K. Weber, O. Romero-Isart, and L. Novotny, Cavity-mediated long-range interactions in levitated optomechanics, *Nat. Phys.* (2024). doi:10.1038/s41567-024-02405-3.
- [65] J. Vijayan, Z. Zhang, J. Piotrowski, D. Windey, F. van der Laan, M. Frimmer, and L. Novotny, Scalable all-optical cold damping of levitated nanoparticles, *Nat. Nanotechnol.* **18**, 49 (2023).
- [66] M. Reisenbauer, H. Rudolph, L. Egyed, K. Hornberger, A. V. Zasedatelev, M. Abuzarli, B. A. Stickler, and U. Delić, Non-Hermitian dynamics and nonreciprocity of optically coupled nanoparticles, arXiv:2310.02610.
- [67] V. Liška, T. Zemánková, P. Jákl, M. Šiler, S. H. Simpson, P. Zemánek, and O. Brzobohatý, Observations of a PT phase transition and collective limit cycle oscillations in non-reciprocally coupled optomechanical oscillators levitated in vacuum, arXiv:2310.03701.
- [68] C. Jakubec, P. Solano, U. Delić, and K. Sinha, Fluctuation-induced forces on nanospheres in external fields, *Phys. Rev. A* **109**, 052807 (2024).
- [69] S. Liu, Z.-q. Yin, and T. Li, Prethermalization and nonreciprocal phonon transport in a levitated optomechanical array, *Adv. Quantum Technol.* **3**, 1900099 (2020).
- [70] A. K. Chauhan, O. Černotík, and R. Filip, Tuneable Gaussian entanglement in levitated nanoparticle arrays, *npj Quantum Inf.* **8**, 151 (2022).
- [71] J. Yan, X. Yu, Z. V. Han, T. Li, and J. Zhang, On-demand assembly of optically-levitated nanoparticle arrays in vacuum, *Photon. Res.* **11**, 600 (2023).
- [72] Y. Bao, S. S. Yu, L. Anderegg, E. Chae, W. Ketterle, K.-K. Ni, and J. M. Doyle, Dipolar spin-exchange and entanglement between molecules in an optical tweezer array, *Science* **382**, 1138 (2023).
- [73] C. M. Holland, Y. Lu, and L. W. Cheuk, On-demand entanglement of molecules in a reconfigurable optical tweezer array, *Science* **382**, 1143 (2023).
- [74] M. M. Burns, J.-M. Fournier, and J. A. Golovchenko, Optical binding, *Phys. Rev. Lett.* **63**, 1233 (1989).
- [75] V. Karásek, K. Dholakia, and P. Zemánek, Analysis of optical binding in one dimension, *Appl. Phys. B* **84**, 149 (2006).
- [76] K. Dholakia and P. Zemánek, Colloquium: Grippled by light: Optical binding, *Rev. Mod. Phys.* **82**, 1767 (2010).
- [77] J. Rieser, M. A. Ciampini, H. Rudolph, N. Kiesel, K. Hornberger, B. A. Stickler, M. Aspelmeyer, and U. Delić, Tunable light-induced dipole-dipole interaction between optically levitated nanoparticles, *Science* **377**, 987 (2022).
- [78] L. Novotny and B. Hecht, *Principles of Nano-optics* (Cambridge University Press, Cambridge, England, 2012).
- [79] M. A. Abbassi and K. Mehrany, Inclusion of the backaction term in the total optical force exerted upon rayleigh particles in nonresonant structures, *Phys. Rev. A* **98**, 013806 (2018).
- [80] D. De Bernardis, G. Rastelli, I. Carusotto, and V. Scarani, Optical-force-mediated coupling between levitated nanospheres can go ultrastrong, arXiv:2203.10126.
- [81] C. W. Gardiner and P. Zoller, *Quantum Noise* (Springer, Berlin, 2000).

- [82] D. Vitali, S. Gigan, A. Ferreira, H. R. Bohm, P. Tombesi, A. Guerreiro, V. Vedral, A. Zeilinger, and M. Aspelmeyer, Optomechanical Entanglement between a Movable Mirror and a Cavity Field, *Phys. Rev. Lett.* **98**, 030405 (2007).
- [83] I. S. Gradshteyn and I. M. Ryzhik, *Table of Integrals, Series, and Products* (Academic, New York, 2014).
- [84] C. Genes, D. Vitali, and P. Tombesi, Simultaneous cooling and entanglement of mechanical modes of a micromirror in an optical cavity, *New J. Phys.* **10**, 095009 (2008).
- [85] Y.-D. Wang and A. A. Clerk, Using Interference for High Fidelity Quantum State Transfer in Optomechanics, *Phys. Rev. Lett.* **108**, 153603 (2012).
- [86] L. Tian, Adiabatic State Conversion and Pulse Transmission in Optomechanical Systems, *Phys. Rev. Lett.* **108**, 153604 (2012).
- [87] D.-G. Lai, J.-F. Huang, X.-L. Yin, B.-P. Hou, W. Li, D. Vitali, F. Nori, and J.-Q. Liao, Nonreciprocal ground-state cooling of multiple mechanical resonators, *Phys. Rev. A* **102**, 011502(R) (2020).
- [88] D.-G. Lai, J.-Q. Liao, A. Miranowicz, and F. Nori, Noise-Tolerant Optomechanical Entanglement Via Synthetic Magnetism, *Phys. Rev. Lett.* **129**, 063602 (2022).
- [89] J. Huang, D.-G. Lai, C. Liu, J.-F. Huang, F. Nori, and J.-Q. Liao, Multimode optomechanical cooling via general dark-mode control, *Phys. Rev. A* **106**, 013526 (2022).
- [90] J. Huang, C. Liu, X.-W. Xu, and J.-Q. Liao, Dark-Mode Theorems for Quantum Networks, arXiv:2312.06274.
- [91] J. Gieseler, L. Novotny, and R. Quidant, Thermal nonlinearities in a nanomechanical oscillator, *Nat. Phys.* **9**, 806 (2013).
- [92] C. Genes, D. Vitali, P. Tombesi, S. Gigan, and M. Aspelmeyer, Ground-state cooling of a micromechanical oscillator: Comparing cold damping and cavity-assisted cooling schemes, *Phys. Rev. A* **77**, 033804 (2008).
- [93] M. Rossi, N. Kralj, S. Zippilli, R. Natali, A. Borrielli, G. Pandraud, E. Serra, G. Di Giuseppe, and D. Vitali, Normal-Mode Splitting in a Weakly Coupled Optomechanical System, *Phys. Rev. Lett.* **120**, 073601 (2018).
- [94] V. Jain, J. Gieseler, C. Moritz, C. Dellago, R. Quidant, and L. Novotny, Direct Measurement of Photon Recoil from a Levitated Nanoparticle, *Phys. Rev. Lett.* **116**, 243601 (2016).